

---

# ~~Sub~~Probabilistic sub-seasonal precipitation forecasts using preceding atmospheric intraseasonal ~~oscillation~~ signals in a Bayesian perspective

Yuan LI<sup>1</sup>, Zhiyong WU<sup>1</sup>, Hai HE<sup>1</sup>, Hao YIN<sup>1</sup>—

5 <sup>1</sup>College of Hydrology and Water Resources, Hohai University, Nanjing 210098, China

Correspondence to: Zhiyong WU ([wzyhhu@gmail.com](mailto:wzyhhu@gmail.com))

**Abstract.** Accurate and reliable sub-seasonal precipitation forecasts ~~remain challenging~~ are of great socioeconomic value for various aspects. The atmospheric intraseasonal oscillation (ISO), which is one of the leading sources of sub-seasonal predictability, ~~could~~can be potentially used as ~~predictors~~predictor for sub-seasonal precipitation forecasts~~...~~. However, the ~~relationships~~relationship between ~~ISO~~atmospheric intraseasonal signals and sub-seasonal precipitation ~~are~~is of high uncertainty. In this study, we ~~first define potential predictors by analyzing the relationship between~~ develop a spatial-temporal projection based Bayesian hierarchical model (STP-BHM) for sub-seasonal precipitation forecasts. The coupled co-variance patterns between preceding atmospheric ~~ISO~~intraseasonal signals and precipitation ~~for 17 hydroclimatic regions~~ are extracted, and the corresponding projection coefficients are defined as predictors. A Bayesian hierarchical model (BHM) is then built to address the uncertainty in the relationship between atmospheric intraseasonal signals and precipitation. The STP-BHM model is applied to predict both pentad mean precipitation amount and pentad mean precipitation anomalies for each hydroclimatic region over China during the boreal summer monsoon season. ~~The Least Absolute Shrinkage and Selection Operator (LASSO) and stepwise regression approaches are used to narrow down the number of potential predictors. A Bayesian hierarchical model is then established to predict sub-seasonal precipitation.~~ The model performance is evaluated through a leave one-year-out cross-validation strategy ~~for both deterministic and probabilistic forecasts~~. ~~The~~ Our results suggest that the ~~statistical model we built in this study could provide skillful deterministic~~STP-BHM model can provide skillful and reliable probabilistic forecasts for both pentad mean precipitation amount and pentad mean precipitation anomalies at leads of 20-25 days over most hydroclimatic regions in China. The results also indicate that the STP-BHM model outperforms the National Centers for Environmental Prediction (NCEP) sub-seasonal ~~precipitation forecasts over southeastern and southwestern~~

10  
15  
20  
25

---

hydroclimatic regions at a to seasonal (S2S) model when the lead time of 20-25 days. However, ~~the deterministic~~ forecast skills are much lower over northeastern China, ~~owing to the underestimation of intraseasonal variability in~~ these regions. ~~The probabilistic~~ is beyond 5 days for pentad mean precipitation amount forecasts ~~are more promising, and the results indicate that the Bayesian hierarchical model could provide skillful and reliable sub-seasonal precipitation forecasts for all hydroclimatic regions from 0-day to 25-day leads.~~ The Intraseasonal signals of 850-hPa and 200-hPa zonal wind (U850 and U200), 850-hPa and 500-hPa geopotential height (H850 and H500) contribute more to the overall forecast skill of pentad mean precipitation amount predictions. In comparison, the outgoing longwave radiation anomalies (OLRA) contribute most to the forecast skill of pentad mean precipitation anomalies predictions. Other sources of sub-seasonal predictability ~~would, such as soil moisture, snow cover, and stratosphere-troposphere interaction, will~~ be included in the future to further improve sub-seasonal precipitation forecast ~~skills~~skill.

---

## 1. Introduction

40 Accurate and reliable sub-seasonal precipitation forecasts can provide vital information for many management  
decisions in water resources, agriculture, and disaster ~~mitigations~~mitigation (Vitart et al., 2012; Vitart and  
Robertson, 2018). One approach for sub-seasonal precipitation forecasts is to run dynamical models such as  
Global Climate Models (GCMs). Projects such as the Subseasonal-to-Seasonal Prediction Project (S2S) and  
the Subseasonal Experiment (SubX) have been ~~lunched~~launched to provide sub-seasonal precipitation  
45 forecasts with lead time up to 60 days from GCMs (Pegion et al., 2019; Vitart et al., 2017). However, the sub-  
seasonal precipitation forecasts derived directly from GCMs are of low accuracy as the physical equations are  
always simplified and small-scale processes ~~could not~~cannot be well represented in the GCMs (De Andrade  
et al., 2019). Post-processing is always required to improve the accuracy and reliability of GCM forecasts  
before it ~~could~~can be used for other applications. Schepen et al. (2018) and our previous study (Li et al., 2020)  
50 used the Bayesian Joint Probability (BJP) method to post-process sub-seasonal precipitation forecasts over  
different regions, and the results suggested that the forecast ~~skills~~skill and reliability were improved compared  
to raw GCM forecasts. Vigaud et al. (2020) proposed a new spatial correction method to improve sub-monthly  
precipitation forecasts derived from multimodel ensembles. Nevertheless, the results also indicated that the  
accuracy of post-processed sub-seasonal precipitation forecasts were still limited when the lead time was  
55 beyond 10-14 days.

An alternative approach for sub-seasonal precipitation forecasts is to establish statistical models based on the  
~~relationships~~relationship between precipitation and preceding atmospheric- or oceanic indices. Although  
dynamical models are ~~dominant~~more performant for short- to medium-term forecasts, statistical models are  
60 still found to be useful especially for long-term forecasts (Tuel and Eltahir, 2018; Abbot and Marohasy, 2014;  
Mekanik et al., 2013; Lü et al., 2011; Kirono et al., 2010). Schepen et al. (2012) suggested that the lagged  
climate indices were potentially useful for seasonal precipitation forecasts over Australia. Plenty of statistical  
algorithms, such as multiple linear regression or canonical correlation analysis, have been developed for  
seasonal precipitation forecasts based on the assumption that the seasonal anomalies are caused by slow-  
65 varying sea surface temperature, sea ice, snow cover, and other boundary conditions (Hwang et al., 2001;  
Barnston and Smith, 1996; Eden et al., 2015). ~~Totz et al. (2017) proposed a new cluster-based empirical  
method to predict winter precipitation anomalies over the European and Mediterranean Regions, which~~A new  
cluster-based empirical method was proposed to predict winter precipitation anomalies over the European and

Mediterranean Regions (Totz et al., 2017). This method used the sea surface temperature, geopotential height, sea level pressure, snow cover extent, and sea ice concentration ~~were included~~ as predictors. A random forest based statistical model, which the predictors were identified from the gridded sea surface temperature, was developed to predict central and south Asia seasonal precipitation (Gerlitz et al., 2016).

However, much fewer statistical models have been built and applied for sub-seasonal precipitation forecasts as the sources of sub-seasonal predictability are not yet fully understood ~~at such a time scale.~~ Compared to seasonal precipitation forecasts, the slow-varying boundary forcings may have limited impact on sub-seasonal precipitation as the time scale is too short. The atmospheric intraseasonal oscillation (ISO), which is the dominant mode of sub-seasonal variability, is one of the leading sources of sub-seasonal predictability (Robertson and Vitart, 2018). The boreal summer intraseasonal oscillation (BSISO) in the tropics, which is also known as Madden-Julian Oscillation (MJO) in winter, is characterized as a slow-moving system with a period of 30-90 days in the tropical atmosphere (Madden and Julian, 1971, 1972; Zhang, 2005; Woolnough, 2019; Wang and Xie, 1997). The circulation anomalies associated with the intraseasonal oscillation (ISO) are identified to have an impact on monsoon activities and heavy rainfall events (Annamalai and Slingo, 2001; Chen et al., 2004). Zhang et al. (2009) found that the rainfall patterns in Southeast China were transitioned from being enhanced to being suppressed when the MJO center moved from the Indian Ocean to the Western Pacific Ocean. Jia et al. (2011) suggested that the MJO influenced the rainfall patterns in China mainly by modulating the circulation in the subtropics and mid-high latitudes in winter. This suggests that the ISO signals could be potentially used for predicting sub-seasonal precipitation not only in tropical regions but in extra-tropical regions as well.

Several statistical models have been built to predict sub-seasonal precipitation based on the ~~relationships between ISO signals and precipitation.~~ relationship between atmospheric intraseasonal signals and precipitation. The spatial-temporal projection (STP) model, which extracts the coupled patterns of predictors and predictand, has been developed in recent years (Hsu et al., 2020; Zhu and Li, 2017a, b, c, 2018). Hsu et al. (2015) established a set of spatial-temporal projection models (STPMs) to predict sub-seasonal precipitation at a lead time of 10-30 days over southern China. Their results suggested that the forecast ~~skills were~~ skill was still promising at a 20-25-day lead time. ~~Zhu and Li (2017)~~ Zhu and Li (2017a) predicted sub-seasonal precipitation by constructing STPMs over entire China, and independent forecasts of rainfall anomalies during the period of Olympic Games in 2008 and Shanghai World Expo in 2010 suggested

100 that the STPMs were able to reproduce intraseasonal rainfall patterns at a 20-day lead time. However, we  
should note that the ~~relationships between ISO signals and precipitation are of high uncertainty for different  
regions at different lead times. Chen and Wang (2021) suggested that different BSISO events would have  
distinct impact on monsoon systems. To our best knowledge, the uncertainties of relationships between  
preceding ISO signals and sub-seasonal precipitation have not been fully considered in sub-seasonal  
precipitation forecasts in previous studies~~relationship between ISO signals and precipitation is highly uncertain  
105 and depend on the region and lead time. In previous studies, an optimal ensemble (OE) strategy was applied  
to generate probabilistic forecasts by picking up best predictors (Zhu and Li, 2017a; Zhu et al., 2015).  
Nevertheless, the number of best predictors was always limited. Further statistical assumptions were required  
to interpret limited ensembles as probabilistic forecasts. The uncertainty in relationship between preceding ISO  
110 signals of atmospheric field and precipitation has not been fully considered yet.

There are several ways to address the above challenge. Lepore et al. (2017) established an extended logistic  
regression model to link the relationship between El Niño-Southern Oscillation (ENSO) and convective storm  
~~(SCS)~~activity. Sohrabi et al. (2021) coupled the large-scale climate indices with a stochastic weather generator  
115 to provide ensemble streamflow forecasts. Compared to the above-mentioned traditional probabilistic model  
solutions, the ~~Bayes theorem based~~Bayesian statistical models are more flexible and more efficient for  
assessing multiple sources of uncertainties. Wang et al. (2009) proposed a multivariate normal distribution  
based Bayesian joint probability (BJP) approach to predict seasonal streamflow over Australia using  
antecedent streamflow, ENSO indices, and other climate indicators as predictors. Peng et al. (2014) utilized  
120 the same BJP approach to predict seasonal precipitation over China using lagged oceanic-atmospheric indices.  
~~Another Bayes theorem based approach, the~~The Bayesian hierarchical model (BHM) has also been  
developed in recent years (Gelman and Hill, 2006). The BHMs are always constructed with several model  
layers. The predictand is assumed to follow distribution with unknown parameters in the first layer, and the  
parameters are linked with the predictors using linear regression models in the second layer. The regression  
125 coefficients are given hyperprior distributions with the BHMs. The utility of BHMs has been demonstrated in  
modelling spatiotemporal variability of hydrological variables in many studies (Renard, 2011; Reza Najafi and  
Moradkhani, 2013; Bracken et al., 2016; Lima and Lall, 2010; Lima and Lall, 2009; Devineni et al., 2013). The  
BHMs are also used for seasonal predictions in many fields. Chen et al. (2014) used the BHM to predict  
summer rainfall and streamflow over the Huai River basin, while Chu and Zhao (2007) developed a BHM  
130 model to predict seasonal tropical cyclone activity over the Central North Pacific. However, the BHMs have not

---

been used to predict sub-seasonal precipitation before. In this study, we follow a similar BHM structure proposed by Devineni et al. (2013) to predict sub-seasonal precipitation.

135 China is located in east Asia, and is frequently ~~influenced by~~subject to rainstorm and flood disasters during the boreal summer monsoon season. Accurate and reliable sub-seasonal precipitation forecasts can provide valuable information for mitigating the risks from rainstorm and flood disasters. However, the origin of intraseasonal precipitation variability is of high complexity owing to the mixed impact of tropical convection, forcing of Tibetan Plateau, and mid-high latitude systems (Zhu and Li, 2017). ~~In this study, we first define potential predictors by analyzing the correlations between preceding ISO signals and precipitation for each hydroclimatic region. In a second step, smaller groups of robust predictors are selected and the Bayesian hierarchical model is established to predict sub-seasonal precipitation. The model performance for both deterministic and probabilistic forecasts are~~(Zhu and Li, 2017a). In this study, we develop a STP-BHM probabilistic forecast model to predict both pentad mean precipitation amount and pentad mean precipitation anomalies over each hydroclimatic region in China during the boreal summer monsoon season. The performance of the STP-BHM model is evaluated through a leave one-year-out cross-validation strategy.

140

145

In the following section, the ~~observations, reanalysis~~ dataset, ~~ISO~~main model components, including intraseasonal signal extraction, ~~potential~~ predictor selection, definition, and Bayesian hierarchical model calibration~~construction~~, and evaluation~~verification methods~~ are introduced. The ~~deterministic and probabilistic~~ forecast ~~skills are~~skill of both pentad mean precipitation amount and pentad mean precipitation anomalies is presented in Sect. 3. Section 4 discusses the forecast ~~skills~~skill, possible mechanism, limitations, and future work. Key findings are summarized in Sect. 5.

150

## 2. Data and Methodology

### 2.1 Data

155 In this study, China is divided into 17 hydroclimatic regions as suggested by Lang et al. (2014). The division is based on both watershed division standard and climate classifications. This will ensure that the climatic characteristics are nearly uniform in each region. The southeastern hydroclimatic regions are mostly of temperate and warm/hot summer climate without dry season (Cfb/Cfa), while the northwestern regions are mostly arid with limited precipitation (Bwk, Bsh, Bsk climate types) (Peel et al., 2007) (Figure 1). The observed

160

precipitation is derived from the Multi-Source Weighted-Ensemble Precipitation, version 2 (MSWEP V2) dataset. The MSWEP V2 dataset is of high spatial (0.1°) and temporal (3 hourly) resolution. Compared to other gridded datasets, the MSWEP V2 exhibits more realistic spatial patterns, and higher accuracy over land (Wu et al., 2018; Beck et al., 2019). The 0.1° gridded precipitation data is area-weighted ~~averaging~~ averaged through 17 hydroclimatic regions over China from May to October. ~~After that, the 3-hourly regional precipitation data is summarized to pentad data to reduce the noise and improve the predictability.~~

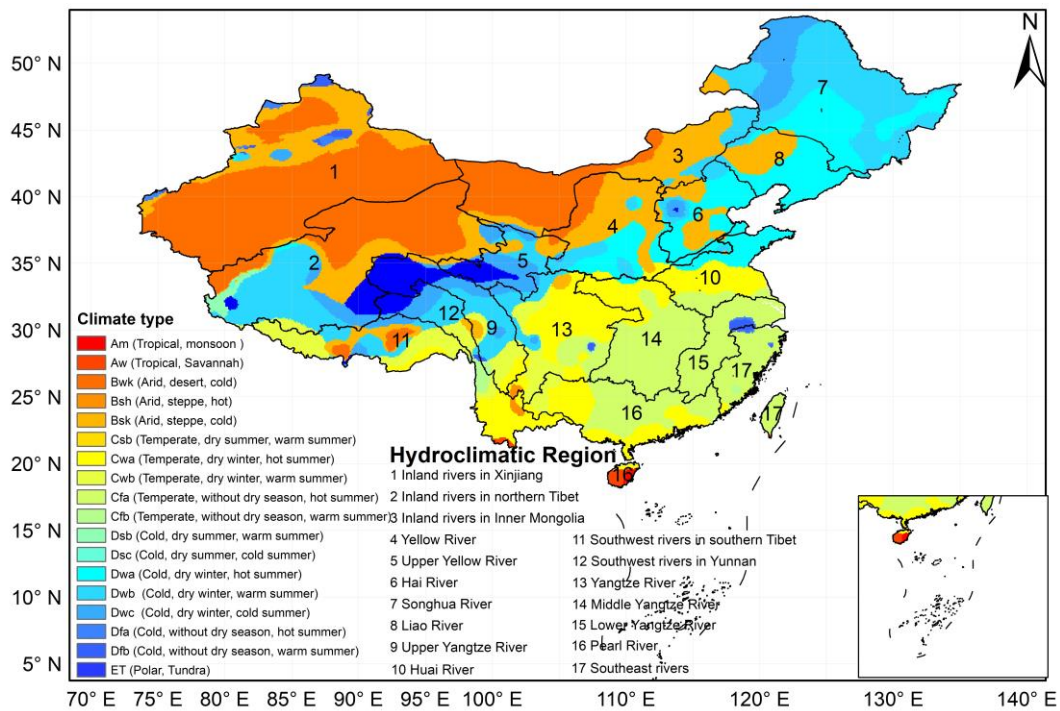


**Figure 1.** 17 hydroclimatic regions over China.

The intraseasonal oscillation is always represented by outgoing longwave radiation (OLR), zonal winds in the upper (200 hPa) and lower (850 hPa) troposphere. Although several indices, including the RMM (Realtime Multivariate MJO) index (Wheeler and Hendon, 2004) and BSISO index (Lee et al., 2013), have been proposed to ~~monitoring~~ monitor the propagation of oscillation, these indices may not cover patterns which might be important for sub-seasonal precipitation in certain regions. To overcome this problem, we analyze the correlation between ~~regional precipitation and ISO signals of~~ preceding global ~~gridded~~ OLR, zonal wind at 850 hPa (U850), zonal wind at 200 hPa (U200) and precipitation for each grid cell. In addition, the correlation between geopotential height at 850 hPa, 500 hPa, and 200 hPa (H850, H500, H200), ~~which~~ are also analyzed. The H850, H500, and H200 have been proved to be as capable of reflecting the MJO structure as the zonal wind (Leung and Qian, 2017), ~~are also analyzed.~~ The OLR daily Climate Data Record (CDR). The OLR data used in this study is derived from National Climate Data Center (NCDC) on a 1.0° squared resolution over the globe. The OLR ~~daily CDR data~~ is developed from high resolution infrared radiation sounder instruments, and

is valuable to a wide range of applications. A more detailed description of the OLR dataset can be found at <https://www.ncdc.noaa.gov/news/new-outgoing-longwave-radiation-climate-data-record>. The global gridded daily average U850, U200, H850, H500, H200 data are derived from the ERA5 reanalysis dataset at <https://cds.climate.copernicus.eu/>. The ERA5 reanalysis dataset is produced using advanced 4D-Var data assimilation scheme, and its horizontal resolution is approximately 30 km with 137 pressure levels in the vertical (Hersbach et al., 2020). It provides hourly record of global atmosphere, land surface and ocean waves from 1950 to present. To focus on large-scale features and increase ~~calculatingcomputational~~ efficiency, both the OLR-~~daily CDR dataset data~~ and the ~~daily average~~ ERA5 reanalysis ~~datasetdata~~ are bilinearly interpolated onto  $2.5^\circ \times 2.5^\circ$  latitude-longitude resolution. Moreover, we choose to focus on the period of 1979-2016 to be consistent with the temporal coverage of observed precipitation data.

The STP-BHM model we built in this study is compared to the dynamical models to provide a benchmark for sub-seasonal precipitation forecasts. However, the dynamical models are not always able to provide pentad mean precipitation forecasts for the same period as the STP-BHM model as the hindcast initial time, hindcast period, and hindcast frequency are different. The comparison may be unfair if the predictand of the statistical model and dynamical models are not the same. To overcome this problem, we compare our results of the STP-BHM model with the NCEP model archived in the S2S Database for the same period of 1999-2010 from May to October (<http://apps.ecmwf.int/datasets/data/s2s/>). The NCEP hindcasts are produced by the Climate Forecast System version 2 (CFSv2), which is composed of land, ocean and atmosphere components. The system provides a 4-member ensemble run every day from 1st January 1999 to 31 December 2010. More details of the NCEP hindcasts are available at <https://confluence.ecmwf.int/display/S2S/NCEP+Model+Description>. The pentad mean precipitation amount forecasts of the NCEP model are generated to be consistent with the STP-BHM model.

## 2.2 Methodology

### 2.2.1 10-60 day ISO signal extraction

#### 2.2.1 Modeling structure

The spatial-temporal projection based Bayesian hierarchical model (STP-BHM) falls into three parts as shown in Figure 2. The first part (Sect. 2.2.2) extracts intraseasonal signals of each global atmospheric field (U850, U200, OLR, H850, H500, and H200) and precipitation using a non-filtering method proposed by Hsu et al. (2015). In the second part (Sect. 2.2.3), the cell-wise correlation between ISO signals of atmospheric field and



precipitation is analyzed in the six preceding pentads. The spatial-temporal coupled co-variance patterns are constructed for grid points where the correlation is statistically significant at the 5% level. The predictor is then defined by summing the product of the co-variance field and atmospheric intraseasonal signals of atmospheric field at each preceding pentad. In the statistical modeling step (Sect. 2.2.4), both predictors and predictand are transformed to follow normal distributions. A Bayesian hierarchical model is then built to address the uncertainty in relationship between the predictors and predictand. The model is applied to generate probabilistic sub-seasonal precipitation forecasts after parameter inference.

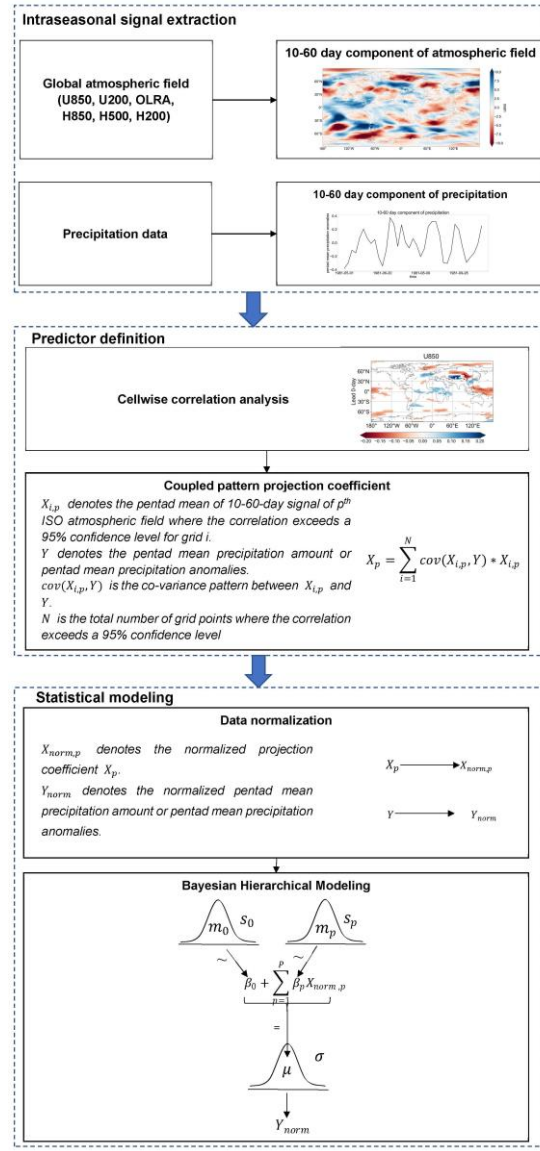


**Figure 2.** workflow of the spatial-temporal projection based Bayesian hierarchical model (STP-BHM).

## 2.2.2 Intraseasonal signal extraction

As briefly introduced in previous section, extracting meaningful ISO intraseasonal signals is important for sub-seasonal precipitation forecasts. However, ~~the~~ high-frequency (unpredictable) noises exist for both raw daily precipitation data atmospheric variables (U850, U200, OLR, H850, H500, and H200) and raw daily large-scale

~~circulation variables-precipitation.~~ Band-pass filtering methods, such as the fast Fourier transformation, ~~should~~  
 225 ~~beare always~~ used to isolate intraseasonal low-frequency (10-60-day) signals from raw data (Zhang, 2005).  
 However, traditional band-pass filtering method is impractical for real time applications as future information  
 beyond the current date is needed. In this study, a non-filtering method proposed by Hsu et al. (2015) is used  
 to extract ~~sub-seasonal component with a period between 10 and 60 days for day signals of~~ both ~~the~~  
~~ISOatmospheric~~ variables and precipitation. Compared to traditional ~~ISOintraseasonal~~ signal extraction  
 230 method, this approach is easy to implement and could be used for real time applications. The climatological  
 annual cycle of raw daily data is first removed by subtracting 90-day low-pass filtered climatological component:

$$x^t = x - \bar{x} \quad X' = X - \bar{X} \quad (1)$$

where  $x^t$  is the ~~areal-weighted raw~~ daily ~~data of atmospheric field or~~ precipitation ~~data for each hydroclimatic~~  
~~region or the gridded large-scale circulation variable U850, U200, OLR, H850, H500, or H200,~~  $\bar{x}$ ,  $\bar{X}$  is the  
 235 corresponding climatological 90-day low-pass filtered component derived by Lanczos filtering method ~~for during~~  
 the period of 1981-2010 (Duchon, 1979). In a second step, lower-frequency signals longer than 60 days are  
 removed by subtracting the last 30-day running mean,

$$x^{tt} = x^t - \overline{x^t}^{30d} \quad X'' = X' - \overline{X'}^{30d} \quad (2)$$

where  $\overline{x^t}^{30d}$ ,  $\overline{X'}^{30d}$  is the last 30-day running mean of  $x^t$ ,  $X'$ .

240 The higher-frequency signals are then removed by taking a pentad mean,

$$x^* = \overline{x^{tt}}^{5d} \quad X^* = \overline{X''}^{5d} \quad (3)$$

~~The so-derived variables represent the 10-60-day component of ISO signals and precipitation.~~

### ~~2.2.2 — Defining potential predictors~~

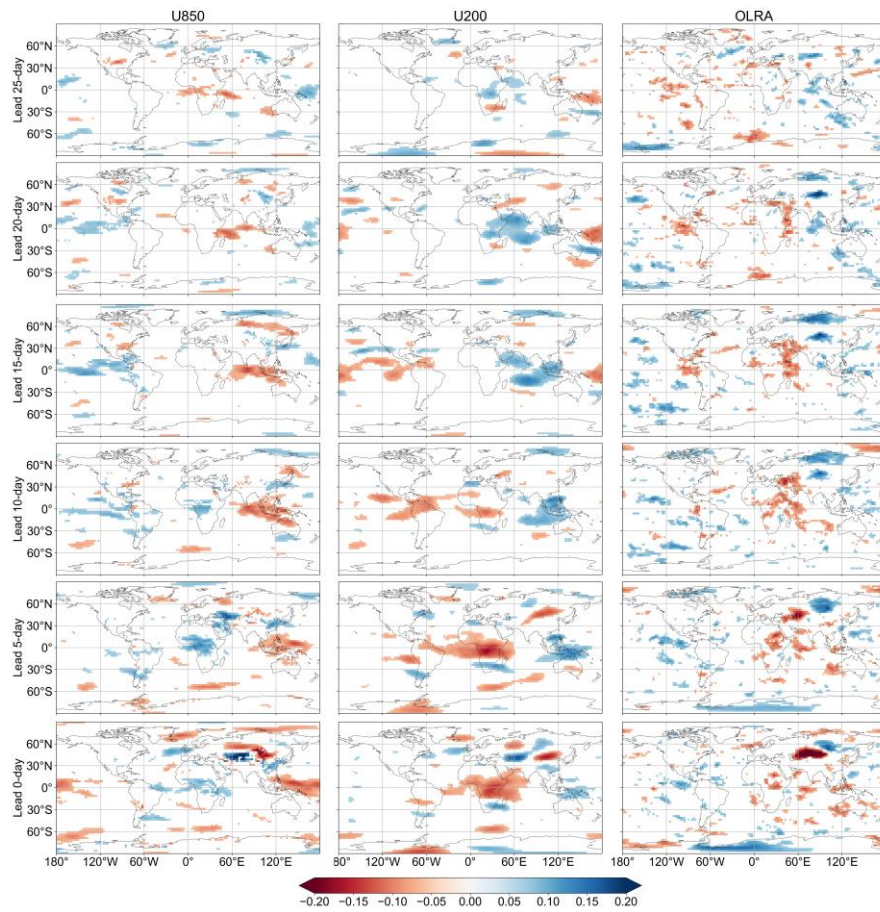
245 ~~The so-derived variable represents the 10-60-day signals of daily atmospheric field or precipitation. The daily~~  
~~intraseasonal signals are then averaged to pentad data to further reduce the noise and improve the~~  
~~predictability. The pentad mean 10-60-day signal of precipitation is also referred as pentad mean precipitation~~  
~~anomalies in the following sections.~~

### ~~2.2.3 Predictor definition~~

250 To identify relevant areas of ~~large-scale circulationatmospheric~~ fields that could affect 10-60-day precipitation  
 variability, we analyze the correlation between ~~extracted ISO signals in the~~ preceding ~~six pentads and~~ 10-60-  
 day ~~componentsignals~~ of ~~atmospheric fields and~~ precipitation for each hydroclimatic region during the period  
 of 1979-2016 ~~from May to October~~. Owing to the data persistence introduced by the filtering method, the

255 effective degree of freedom for each grid cell and each preceding pentad is estimated following Livezey and  
Chen (1983). ~~The identified significantly correlated preceding ISO signals are then used to establish the  
Bayesian hierarchical model to produce a 0-25 day lead time precipitation forecasts.~~

260 As an example, Figure 23 and Figure 4 presents the correlation between preceding pentad mean 10-60-day  
signals of U850, U200, OLROLRA, H850, H500, H200 and 10-60-day component of precipitation over Region  
1 (Inland Rivers in Xinjiang) at different lead times. At leads 25 to 20 days, the significantly correlated U850  
signals are mainly over the Arabian Sea and the Bay of Bengal-western Indian Ocean. The U850 signals are  
then propagating eastward toward South China Sea and Philippine Sea Equatorial Indian Ocean at the lead of  
15 to 10 days. The U850 anomalies then gradually moved eastward and northward toward West Pacific Ocean,  
Mongolia plateau, Iranian plateau, and Qinghai-Tibet plateau from the lead of 10 to 0 days. The U200 ~~ISO~~  
265 signals are more pronounced compared to U850 signals. The spatial distribution of potential predictive U200  
regions is rather concentrated, indicating more robust statistical relationships. The OLR anomalies appear  
near the Indian Ocean Bay of Bengal at 20 to 15 day leads. At lead 5 to 0 day, the significantly correlated OLR  
signals are mainly over the East European Plain and West Siberian Plain.



270

**Figure 3.** Correlation coefficient between preceding pentad mean 10-60-day signals of U850, U200, OLRA and precipitation over Region 1 (Inland Rivers in Xinjiang) at different lead times during the period of 1979~2016 from May to October. Correlation coefficients statistically significant at the 5% level are shaded.

275 The H850 and H500 high anomalies appear near the Africa, equatorial Indian Ocean and Philippine Sea at the lead of 25 days to 20 days to 15 days, and. At leads 15 to 20 days, the significantly correlated H850 signals are mainly over Africa. The signals gradually move eastward and northward toward Indian Ocean, Iranian plateau, and Central Asia from the lead of 10 to 0 days. Unlike the H850 and H500 fields that originated over the Africa, the H200 anomaly appears to originate from the Arabian Sea, southern Indian Ocean, and West Pacific Ocean from leads of 25 to 15 days. At lead 10 to 0 days, the significantly correlated H200 signals are mainly over the East European Plain, West Siberian Plain, and Central Siberian plateau.

280

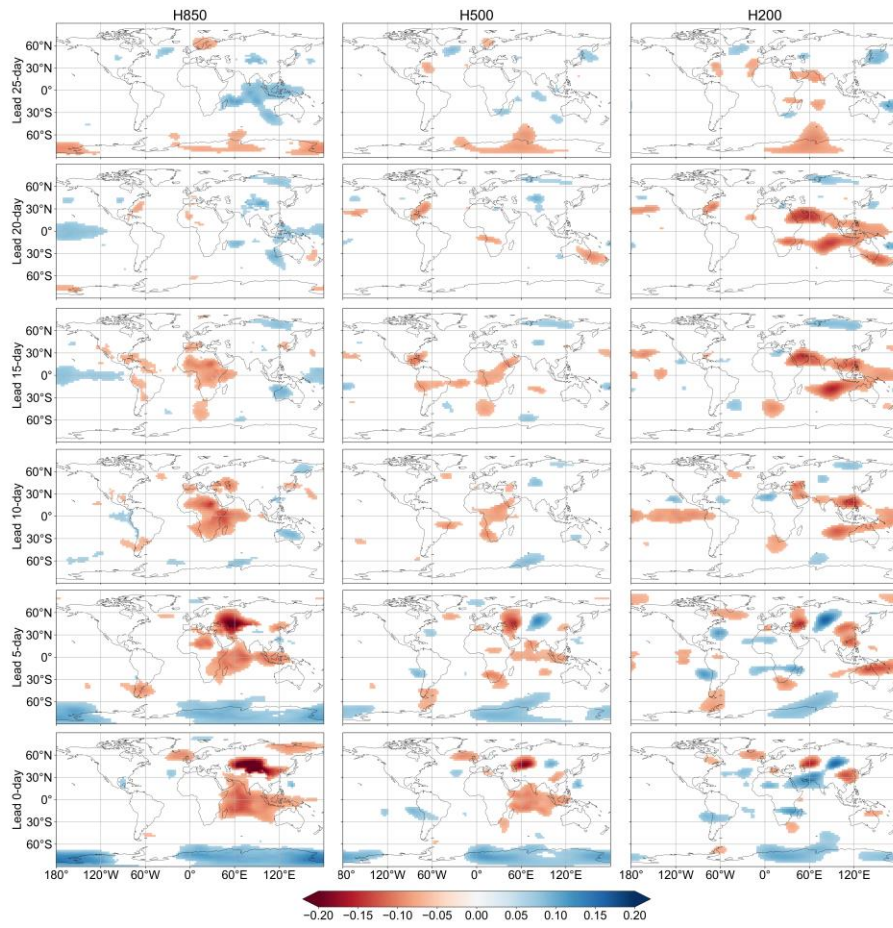


**Figure 4.** Same as Figure 3, but for H850, H500, and H200.

The correlation maps

285 To avoid defining too many predictors, which would lead to overfitting, we define potential predictors by averaging U850, U200, OLR, H850, H500, H200 signals in the areas of significant correlations at different lead times. The irregular boundaries of significant correlated areas are identified by the Python package scikit-

image (Walt et al., 2014). A total number of about one or two dozen potential predictors are defined for each hydroclimatic region and each preceding pentad.

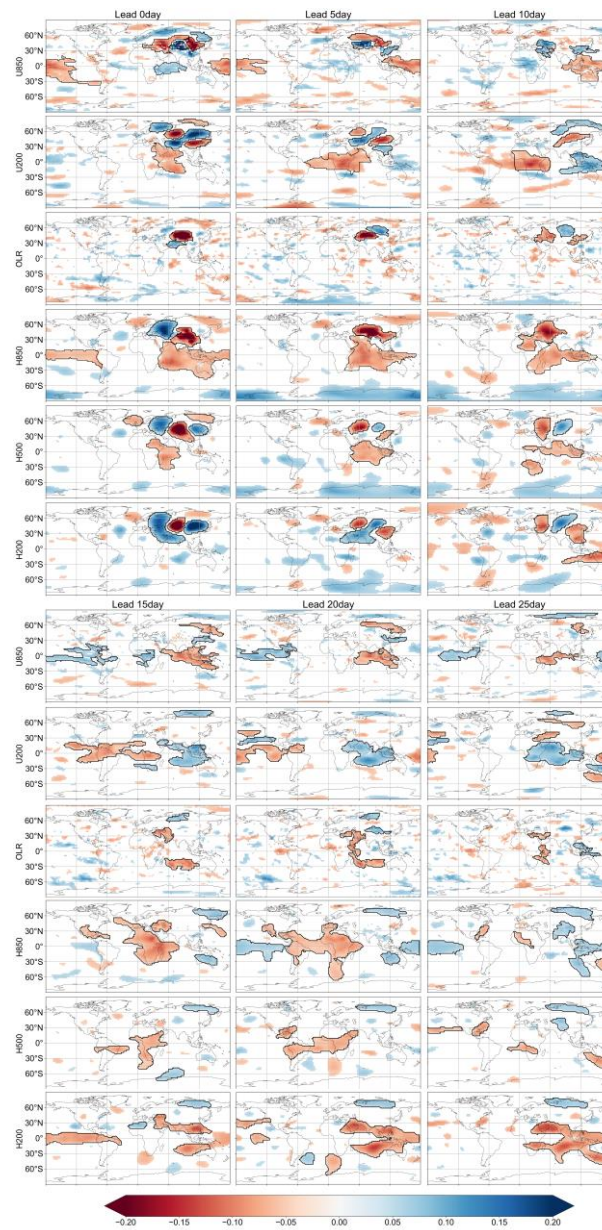


**Figure 2.** Correlation between preceding ISO pentad mean 10-60-day signals of U850, U200, OLR, H850, H500, H200 and 10-60-day component of precipitation over Region 1 (Inland Rivers in Xinjiang) other regions are presented in Figures S1 to S32.

The spatial-temporal coupled co-variance patterns are then constructed for grid point where the correlation statistically significant at the 5% level. The predictor is then defined by summing the product of the co-variance patterns and ISO signals of atmospheric field at different lead times. Correlation coefficients each preceding pentad.

$$cov(X_{i,p}, Y) = \frac{1}{T} \sum_{t=1}^T (y_t - E(y))(x_{i,p,t} - E(x_{i,p})) \quad (4)$$

$$X_p = \sum_{i=1}^N cov(X_{i,p}, Y) * X_{i,p} \quad (5)$$

where  $X_{i,p}$  denotes the pentad mean 10-60-day signal of  $p^{th}$  atmospheric field where the correlation statistically significant at the 5% level ~~are shaded~~ for grid  $i, p = 1, 2, \dots, 6$ .  $Y$  denotes the pentad mean precipitation amount or pentad mean precipitation anomalies.  $T$  is the total number of pentads, and  $N$  is the total number of grid points where the correlation statistically significant at the 5% level. Thus, there is only one predictor  $X_p$  for each atmospheric field and each preceding pentad.

#### **2.2.32.2.4 Statistical modelling**

In previous steps, we defined ~~potential~~ predictors by analyzing the relationship between ISO signals of atmospheric field and ~~10-60-day component of~~ precipitation. The so-derived predictors ~~could~~ can be used to predict ~~sub-seasonal precipitation amount as well as precipitation indices~~ (Li et al., 2016; Leung and Qian, 2017). Here, the defined predictors are used to predict pentad mean precipitation amount as ~~it could also be used for hydrological applications well as pentad mean precipitation anomalies~~. Consider, for example, predicting pentad mean precipitation amount for the period between 4<sup>th</sup> 1<sup>st</sup> May and 5<sup>th</sup> May, 1979. In this case, pentad mean ISO signals ~~extracted of atmospheric field~~ on 26<sup>th</sup>~30<sup>th</sup> April, 21<sup>th</sup>~25<sup>th</sup> April, 16<sup>th</sup>~20<sup>th</sup> April, 11<sup>th</sup>~15<sup>th</sup> April, 6<sup>th</sup>~10<sup>th</sup> April, 1<sup>st</sup>~5<sup>th</sup> April 1979 are used as predictors to ~~produce~~ generate precipitation forecasts at different lead times. A leave-one-year-out cross-validation strategy is implemented for both ~~potential predictor selection, data~~ normalization, model building, parameter inference, and verification to avoid any bias in skill (Michaelsen, 1987). For instance, to produce sub-seasonal precipitation forecasts in 1979, the predictors (preceding ISO signals) and predictand (pentad mean precipitation) during the period of 1980-2016 are pooled together for statistical modelling. The forecasts for the year 1979 are then issued by models trained on 1980-2016, and the performance is evaluated against the observations. This cross-validation strategy ensures that the data used for evaluation is never used for statistical modelling.

**Before establishing the Bayesian hierarchical model, the predictors  $X^T = [X_1 X_2 \dots X_p]$  are normalized to  $X_{norm}^T = [X_{norm,1} X_{norm,2} \dots X_{norm,p}]$  through the Yeo-Johnson transformation method as the input variables are allowed to be negative (Yeo and Johnson, 2000). Potential predictor selection**

~~The number of potential predictors defined previously is still too large for statistical modelling. To narrow down the number of potential predictors, we first use the Least Absolute Shrinkage and Selection Operator (LASSO)~~

330 regression to select a smaller subset of robust potential predictors. LASSO is a regularization method that reduces the absolute value of large coefficients. It has been proved to be efficient in selecting predictors and reducing model complexity in many fields (Hammami et al., 2012; Chu et al., 2020). A detailed description of LASSO could be found in (Nardi and Rinaldo, 2011; Mcneish, 2015). After that, we utilize a combined forward and backward variable selection process, which is also known as the stepwise regression, to further select the  
 335 most informative predictors for each hydroclimatic region and each preceding pentad.

### Bayesian hierarchical model framework

Before establishing the Bayesian hierarchical model, we standardize and normalize the pentad mean precipitation data  $V_{s,t}$  over Region  $s$  at the lead time of  $t$  to  $V_{s,t}^T$ . The predictand  $Y$  is normalized to  $Y_{norm}$   
 340 using the Yeo-Johnson method for pentad mean precipitation anomalies. However, the pentad mean precipitation amount is highly skewed with numerous zero values. Here, we normalize the pentad mean precipitation amount  $Y$  to  $Y_{norm}$  using the log-sinh transformation method proposed by Wang et al. (2012). The zero values of pentad mean precipitation are treated as censored data. The selected preceding potential predictors  $X_{s,t}^T = [X_{1,s,t}, X_{2,s,t}, \dots, X_{n,s,t}]$  are standardized and normalized to  $U_{s,t}^T = [U_{1,s,t}, U_{2,s,t}, \dots, U_{n,s,t}]$  through  
 345 the Yeo-Johnson transformation method as the input variables are allowed to be negative (Yeo and Johnson, 2000). The normalization parameters are estimated using the SCE-UA (shuffled complex evolution method developed at The University of Arizona) method that maximize the log-likelihood function. A more detailed description of the log-sinh normalization method can be found in Wang et al. (2012), for both the Yeo-Johnson transformation method and log-sinh transformation method.

350 There are many versions and variations of BHMs. In this study, we establish the BHM model following Devineni et al. (2013) and Chen et al. (2014). However, the spatial correlation of precipitation over different regions is not considered here. A traditional no-pooling BHM is built for each hydroclimatic region separately. Meanwhile, the potential predictors have been selected using the LASSO and stepwise regression previously. This indicates that the predictors used for establishing the BHM are independent. Thus, it is reasonable to model the related regression coefficients in the BHM independently. The transformed pentad mean precipitation  $V_{s,t}^T$ . The normalized predictand  $Y_{norm}$  is assumed to follow the normal distribution,

$$V_{s,t}^T Y_{norm} \sim N(\mu_{s,t}, \sigma_{s,t}^2) \quad (46)$$

We then link the parameter  $\mu_{s,t}$  with the normalized predictors using a linear model,

$$\mu_{s,t} = \beta_{0,s,t} + \sum_{i=1}^n \beta_{i,s,t} U_{i,s,t} \quad (5)$$

$$\mu = \beta_0 + \sum_{p=1}^P \beta_p X_{norm,p} \quad (7)$$

where  $\beta_{t,s,t} \beta_p$  is the slope term for Region  $s$  at the lead time of  $t$  corresponding to the normalized predictor  $U_{t,s,t}$ . This indicates that the regression coefficients are modeled independently  $X_{norm,p}$  and  $P$  is the total number of predictors used for prediction.

365

To complete the hierarchical formulation, we assume the unknown parameters, including  $\sigma_{s,t}, \sigma_{t,s,t}, \beta_{0,s,t}, \dots, \beta_{n,s,t} \beta_p$ , follow non-informative priors:

$$\frac{1}{\sigma_{s,t}^2} \sim U(0, 100) \quad (68)$$

$$\beta_{t,s,t} \beta_0 \sim N(0, 10^4) \quad (9)$$

370

$$\beta_p \sim N(0, 10^4), \quad i = 0, \dots, n \quad (7p = 1, \dots, P) \quad (10)$$

This implies that the information used for posterior distribution inference is only provided by the data.

Given  $\theta = \{(\sigma_{s,t}, \sigma_{t,s,t}, \beta_{t,s,t}), i = 0, \dots, n, \beta_0, \beta_p, p = 1, \dots, P\}$  denotes parameters in the Bayesian hierarchical model for Region  $s$  at the a certain region and lead time  $t$ ,  $V$  denotes the normalized pentad mean precipitation data, and  $U$  denotes the normalized preceding predictors, the full posterior of the parameters is given as:

375

$$p(\theta | U, V) \propto p(V | Y_{norm}, X_{norm}^T) \propto p(Y_{norm} | \theta, U) X_{norm}^T p(\theta) \quad (811)$$

where  $p(V | Y_{norm}, \theta, U) X_{norm}^T$  is the likelihood, and  $p(\theta)$  is the prior of parameters  $\theta$ . As the posterior distributions of parameters  $\theta$  are not standard distributions, it is difficult to conduct analytical integration. In this study, we use the R package *runjags* (Denwood, 2016) to calibrate/estimate the parameters of the BHM. The *runjags* offers an interface to facilitate calibrating BHM employ a Gibbs sampling algorithm in Just Another Gibbs sampler (JAGS). The initial values of model parameters  $\theta$  are first randomly sampled from prior distributions. The parameters  $\theta$  are then updated based on the full conditional distributions. We use five independent Markov chains in each model run, with a total number of 10, 000 iterations for each chain. The convergence is ensured by the potential scale reduction factor  $\hat{R}$  (Brooks and Gelman, 1998). An approximate convergence is diagnosed when the  $\hat{R}$  is less than 1.1 for all parameters.

385

Once the parameters are sampled, the Bayesian hierarchical model can be used to forecast sub-seasonal/predict pentad mean precipitation amount or pentad mean precipitation anomalies using preceding large-scale circulation/ISO signals. Given new preceding predictors  $X_{s,t}^* = [X_{1,s,t}^* \dots X_{n,s,t}^*]^T$  at the lead time of  $t$ ,  $X^{*T} = [X_1^* X_2^* \dots X_P^*]$ , the normalized predictors  $U_{s,t}^* = [U_{1,s,t}^* \dots U_{n,s,t}^*]^T X_{norm}^{*T} = [X_{norm,1}^* X_{norm,2}^* \dots X_{norm,P}^*]$  are

390



found using the estimated transformation parameters during the training period. The posterior predictive distribution of normalized pentad mean precipitation predictand is given as:

$$V_{s,t}^* Y_{norm}^* \sim N(\mu_{s,t}^*, \sigma_{s,t}^2) \quad (912)$$

$$\mu_{s,t}^* = \beta_{0,s,t} + \sum_{i=1}^n \beta_{i,s,t} U_{i,s,t}^* \quad (10)$$

$$\mu^* = \beta_0 + \sum_{p=1}^P \beta_p X_{norm,p}^* \quad (13)$$

Again, the Gibbs sampling algorithm is used to obtain samples of  $V_{s,t}^* Y_{norm}^*$  by given giving each of the 1000 sets of parameter value sets  $\theta$  values  $\theta$ . The samples of  $V_{s,t}^* Y_{norm}^*$  are then back-transformed to produce ensemble precipitation forecasts of  $Y_{s,t}^*$  over Region  $s$  at the lead time of  $t$ .  $Y^*$ .

## 2.2.4 Deterministic and Probabilistic Evaluation

The deterministic sub-seasonal precipitation forecast skills are evaluated using

## 2.2.5 Verification

In this study, we assess the Kling-Gupta Efficiency (KGE):

$$KGE = 1 - \sqrt{(r-1)^2 + (\beta-1)^2 + (\gamma-1)^2} \quad (11)$$

$$r = \frac{\sum_{i=1}^N (y_i - \bar{y})(o_i - \bar{o})}{\sqrt{\sum_{i=1}^N (y_i - \bar{y})^2} \sqrt{\sum_{i=1}^N (o_i - \bar{o})^2}} \quad (12)$$

$$\beta = \frac{\mu_{\bar{y}}}{\mu_{\bar{o}}} \quad (13)$$

$$\gamma = \frac{\sigma_{\bar{y}}}{\sigma_{\bar{o}}} \quad (14)$$

where  $y_i$  is the ensemble mean forecasts for case  $i$ ,  $i = 1, 2, \dots, N$ ;  $o_i$  is the corresponding observation.  $\mu_{\bar{y}}$  is the forecast mean for all cases; while  $\mu_{\bar{o}}$  is the observation mean for all cases.  $\sigma_{\bar{y}}$  is the standard deviation in ensemble mean forecasts; while  $\sigma_{\bar{o}}$  is the standard deviation in observations.  $r$  represents the correlation coefficient between ensemble mean forecasts and the observations,  $\beta$  represents the forecast bias, and  $\gamma$  measures the variability error. Compared with other evaluation metrics, the KGE offers an insight into the model performance as the decomposition into correlation, bias, and variability term. A full discussion of the KGE statistics sees Gupta et al. (2009) and Kling et al. (2012). The KGE ranges from negative infinity to one. A value of one suggests that the ensemble mean forecasts are the same as the observations.

STP-BHM model for both pentad mean precipitation amount and pentad mean precipitation anomalies. The Continuous Ranked Probability Score (CRPS) is used to provide an overall evaluation of the accuracy of probabilistic sub-seasonal forecasts for both the pentad mean precipitation forecasts amount and pentad mean precipitation anomalies:

$$CRPS_{CRPS} = \frac{1}{N} \sum_{i=1}^N \int [F_i(y) - H(y - o_i)]^2 dy \quad (4514)$$

where  $F_i()$  is the cumulative distribution function of the ensemble forecasts for pentad mean precipitation amount or pentad mean precipitation anomalies for case  $i$ ; and  $H()$  is the Heaviside step function defined as:

$$H(y - o_i) = \begin{cases} 0 & y < o_i \\ 1 & y \geq o_i \end{cases} \quad (4615)$$

425 where  $o_i$  is the corresponding observation.

The CRPS skill score is then calculated by comparing the CRPS of ensemble forecasts with the CRPS of reference forecasts:

$$CRPS_{SS} = \frac{CRPS_{REF} - CRPS}{CRPS_{REF}} \quad CRPS_{SS} = \frac{CRPS_{REF} - CRPS}{CRPS_{REF}} \times 100\% \quad (4716)$$

430 The reference forecasts are generated using the Bayesian hierarchical model with no predictors used for prediction. This is also referred as the cross-validated climatology. A skill score of 100% indicates that the ensemble forecasts are the same as the observations, whereas a skill score of 0% suggests that the ensemble forecasts show no improvement over the cross-validated climatology. A negative skill score means that the ensemble forecasts are inferior to the cross-validated climatology.

435

We also use the Brier Score (BS) to assess the capability of the STP-BHM model for predicting below-normal and above-normal events. The below-normal and above-normal events are defined using the terciles of pentad mean precipitation amount or pentad mean precipitation anomalies of cross-validated climatology.

$$BS = \frac{1}{N} \sum_{i=1}^N (p_i - o_i)^2 \quad (17)$$

440 where  $p_i$  is the forecast probability of the below- or above-normal event for case  $i$ ; and  $o_i$  is the observed occurrence (0 or 1).

The Brier skill score (BSS) is then calculated as follows:

$$BSS = \frac{BS_{REF} - BS}{BS_{REF}} \times 100\% \quad (18)$$

445 where the  $BS_{REF}$  is the  $BS$  of the cross-validated climatology. The  $BSS$  measures the relative skill of the forecast compared to climatology. Like the CRPS skill score, the Brier skill score takes the value 100% for perfect forecasts and 0% for the cross-validated climatology.

In this study, we use the attribute diagram ~~is used here~~ to ~~evaluate~~ assess the reliability, resolution, and sharpness of ~~the~~ probabilistic forecasts for both below-normal event and above-normal event. The attribute

450 diagram shows the observed frequencies against its forecast probabilities for a given event with binary outcomes (Hsu and Murphy, 1986). ~~In this study, the three class events of below, near, and above normal is defined by equally dividing the cross-validated climatology into terciles.~~ The forecast probability is binned as 5 equal-width intervals, which are [0.0, 0.2), [0.2, 0.4), [0.4, 0.6), [0.6, 0.8), and [0.8, 1.0]. The corresponding observed relative frequency is plotted against the mean forecast probability in each bin. The forecasts are reliable if the scatters are along the 45-degree diagonal. The sharpness is also shown on the attribute diagram. 455 The forecasts are sharp if the probabilities tend to be either very high (e.g. > 90%) or very low (e.g. <10%) (Peng et al., 2014). ~~The~~ The size of each dot represents the fraction of forecasts that fall into a particular probability bin. Thus, the sharpness is indicated by the size of dots in each bin. The attribute diagram requires a large number of samples to draw robust conclusions. In this study, the probabilistic forecasts over the 17 460 hydroclimatic regions are pooled together to increase the sample size for each lead time.

### 3. Results

#### 3.1 Deterministic forecast skill

465 ~~Figure 3 summaries the KGE values for all regions and all lead times. Skillful deterministic sub-seasonal precipitation forecasts are observed mainly in regions in southeastern and southwestern China. The KGE values are above 0.2 over Region 2 (Inland Rivers in northern Tibet), Region 9 (Upper Yangtze River), Region 11 (Southwest Rivers in Southern Tibet), Region 12 (Southwest Rivers in Yunnan), Region 13 (Yangtze River), and Region 16 (Pearl River) for almost all lead times. Although the KGE values are lower in Region 1 (Inland Rivers in Xinjiang), Region 7 (Songhua River), Region 14 (Middle Yangtze River), Region 15 (Lower Yangtze River), and Region 17 (Southeast Rivers), positive KGE values still can be found when the lead time is beyond 40 days. This indicates that the deterministic forecasts still can provide useful information at longer lead times over these regions. Much lower predictive skills are observed in northern and northeastern regions, that is Region 3 (Inland Rivers in Inner Mongolia), Region 4 (Yellow River), Region 5 (Upper Yellow River), Region 6 (Hai River), Region 8 (Liao River), and Region 10 (Huai River). The KGE values over these regions are near or below zero when the lead time is beyond 5 days.~~

470

475

~~Figure 4 shows the ensemble mean forecasts during the period of 1979~2016, alongside 50% and 95% confidence intervals from the Bayesian hierarchical model over Region 1 (Inland Rivers in Xinjiang) at different lead times. The positive KGE values suggest that the established Bayesian hierarchical model can provide~~

skillful deterministic precipitation forecasts up to 25 days ahead for Region 1. The correlation coefficient  $r$  is always above 0.35, the biases are below 20% for all lead times. However, we should also note that the variability ratio  $\gamma$  is below 0.5 when the lead time is beyond 5 days. This suggests that the observed precipitation variability is underestimated for ensemble mean forecasts.

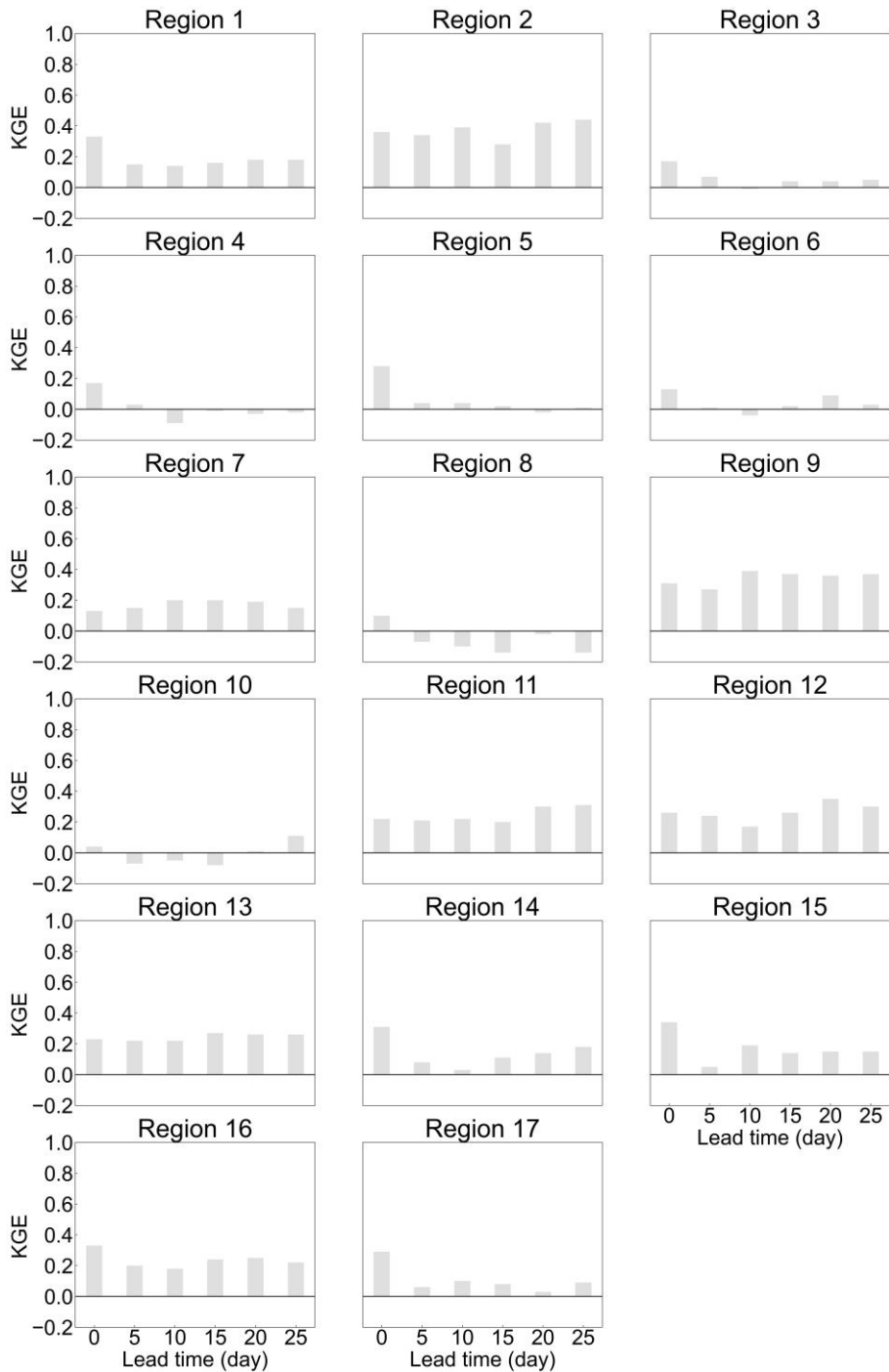
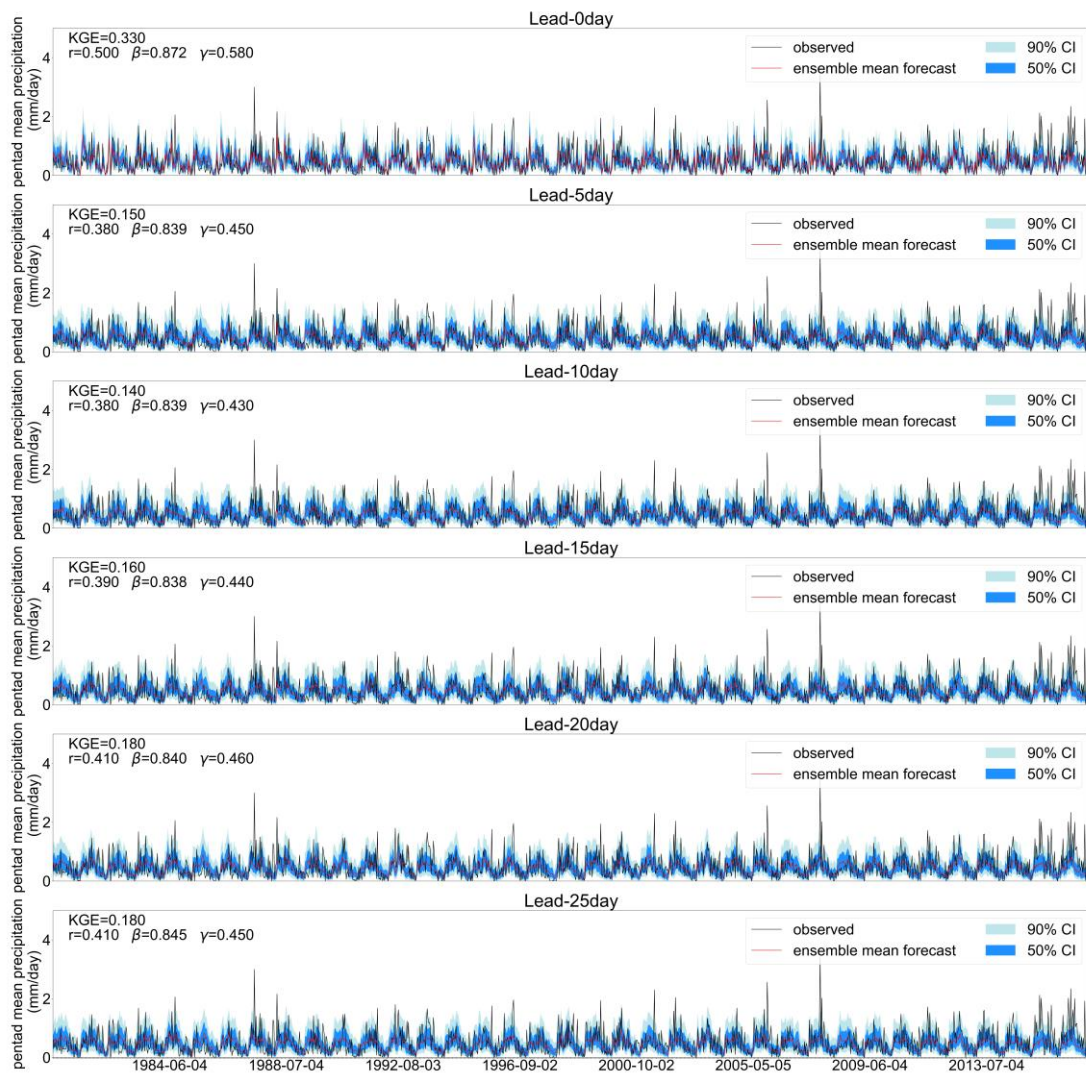


Figure 3. Kling-Gupta Efficiency of Pentad mean precipitation forecasts at different lead times over 17 hydroclimatic regions during the boreal summer monsoon.

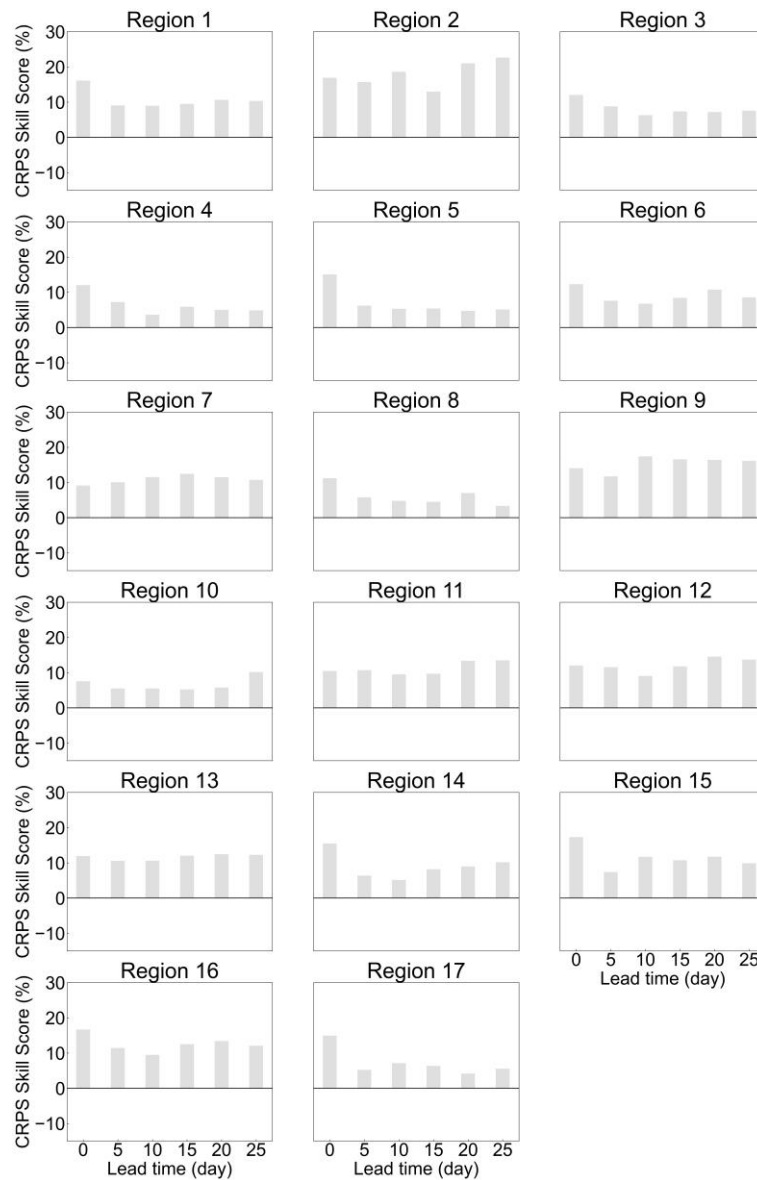


490 **Figure 4. Pentad mean precipitation forecasts at different lead times over Region 1 (Inland Rivers in Xinjiang) during the boreal summer monsoon from 1979 to 2016. The ensemble mean forecasts are shown by the red line, observations by the black line, alongside 50% (shaded in blue) and 95% (shaded in powderblue) confidence intervals. CI – confidence interval.**

495 **3.2 Probabilistic forecast skill**

The positive CRPS skill scores shown in Figure 5 suggest that the Bayesian hierarchical model is able to provide skillful probabilistic forecasts for all regions and all lead times. The CRPS skill scores are mostly over 10% over regions where positive KGE values are observed, including Region 2 (Inland Rivers in northern Tibet), Region 9 (Upper Yangtze River), Region 11 (Southwest Rivers in Southern Tibet), Region 12 (Southwest Rivers in Yunnan), Region 13 (Yangtze River), and Region 16 (Pearl River). Although the KGE values are negative over Region 3 (Inland Rivers in Inner Mongolia), Region 4 (Yellow River), Region 5 (Upper Yellow River), Region 6 (Hai River), Region 8 (Liao River), and Region 10 (Huai River) when the lead time is beyond

5 days, the positive CRPS skill scores suggest that the probabilistic forecasts still can provide valuable information compared to climatological forecasts at longer lead times.



505

Figure 5. Continuous Ranked Probability Skill Score of Pentad mean precipitation forecasts at different lead times over 17 hydroclimatic regions during the boreal summer monsoon.

### 3.1 Attribute diagrams of Forecast skill of pentad mean precipitation amount

510

Figure 5 presents the cross-validated CRPS skill scores for sub-seasonal forecasts of pentad mean precipitation amount at different lead times (lag times). Positive CRPS skill scores are found over all regions and all lead times, indicating that the STP-BHM model outperforms the cross-validated climatological forecasts. The CRPS skill scores are mostly over 10% in southern China even when the lead time is beyond 10 days. On the contrary, the performance of the STP-BHM model is relatively poorer

515

in northern China with CRPS skill scores ranging from 5% to 10% at the same lead time.

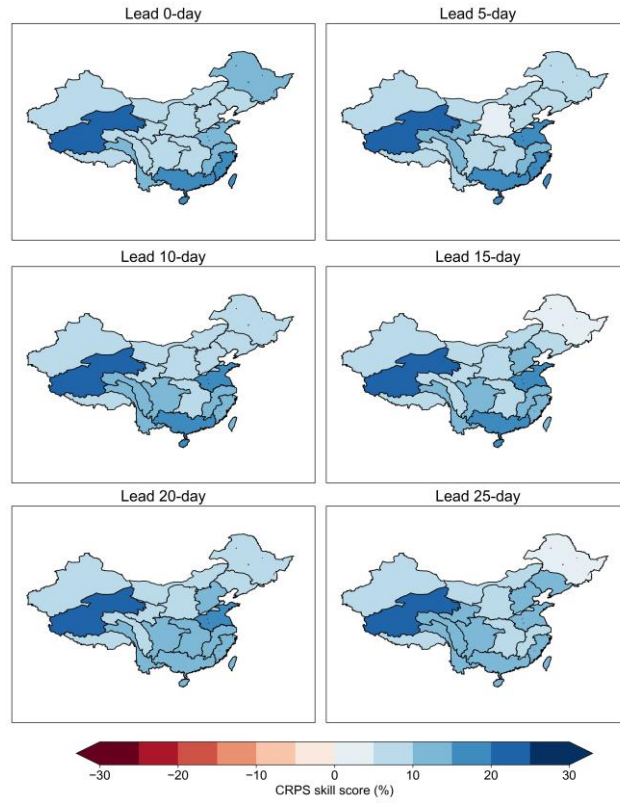
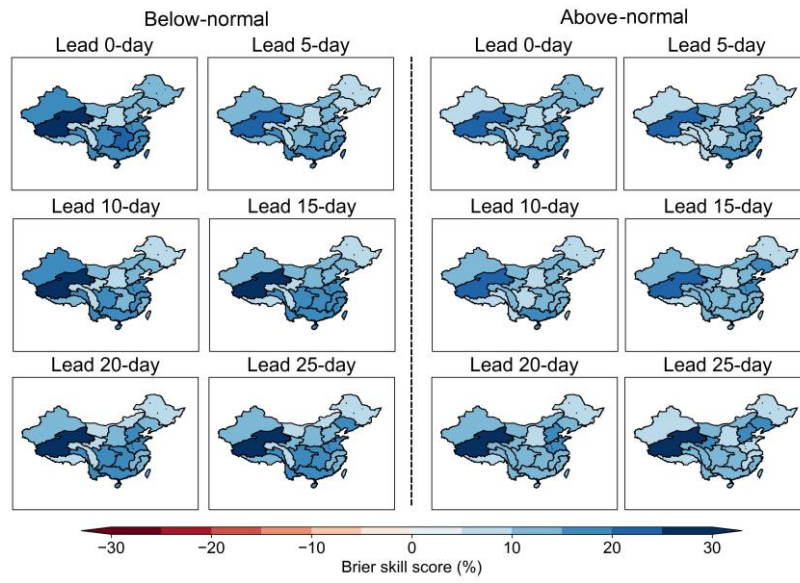


**Figure 5.** The cross-validated CRPS skill scores of the sub-seasonal STP-BHM model for pentad mean precipitation probabilistic amount forecasts at different lead times during the period of 1979-2016 from May to October.

520

Figure 6 illustrates the brier skill scores of the STP-BHM model for both below-normal and above-normal events at different lead times. As can be seen in Fig. 6, the brier skill scores are mostly above 15% for both the below-normal and above-normal events. This indicates that the STP-BHM model can provide skillful sub-seasonal forecasts for extreme events as well. Furthermore, the brier skill scores are most ranging from 20% to 25% in southern China at leads of 20-25 days for below-normal events. The STP-BHM model shows lower forecast skills for above-normal events, which the brier skill scores are mostly between 15% and 20%. This indicates that the below-normal events are more predictable compared to the above-normal events.

525



530 **Figure 6.** The Brier skill scores of the STP-BHM model for the prediction of below-normal and above-normal events of pentad mean precipitation amount at different lead times during the period of 1979-2016 from May to October.

535 To help identify the main sources of sub-seasonal precipitation predictability, we also establish the STP-BHM model for each atmospheric field separately. Figure 7 compares the CRPS skill scores of pentad mean precipitation forecasts with different predictors. In general, U850, U200, H850, and H500 show higher forecast skill compared to OLRA and H200 for almost all hydroclimatic regions and lead times. This suggests that the ISO signals of these atmospheric fields contribute more to the overall forecast skill. Compared to the STP-BHM model built with only one predictor, the forecast skill is further improved when

540 all ISO signals of atmospheric fields are used.



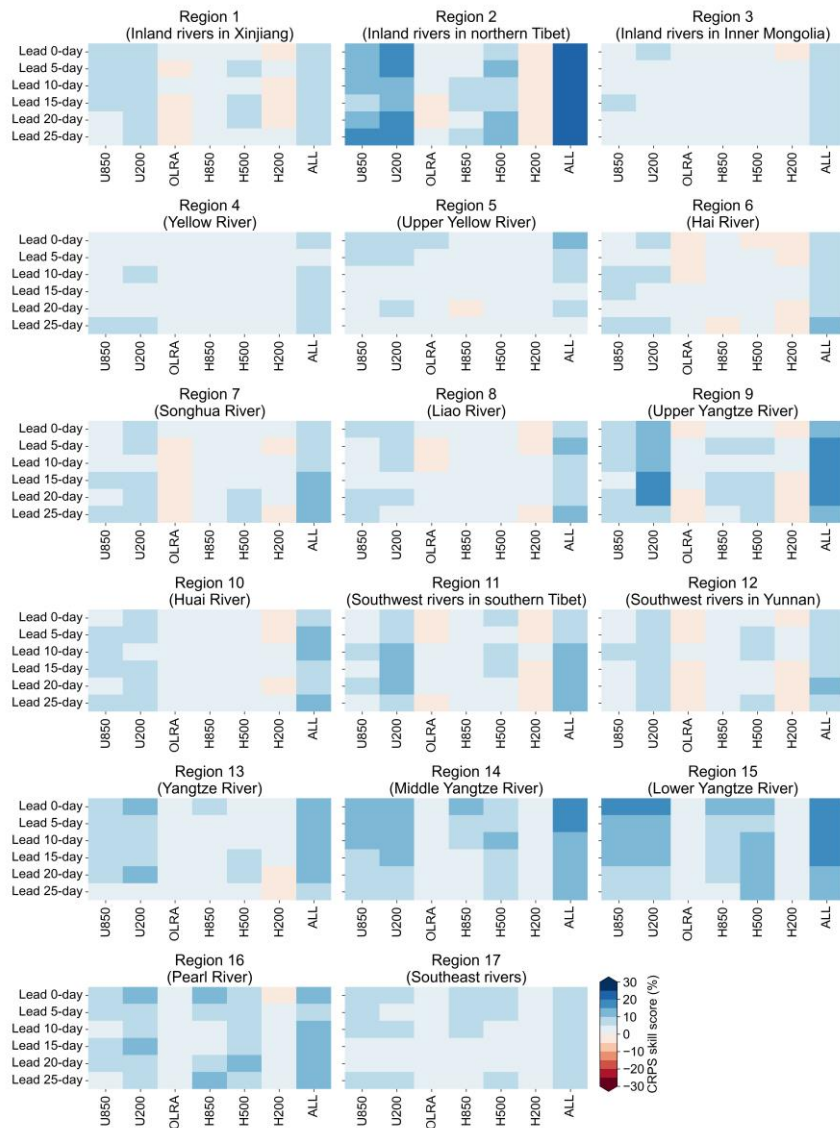
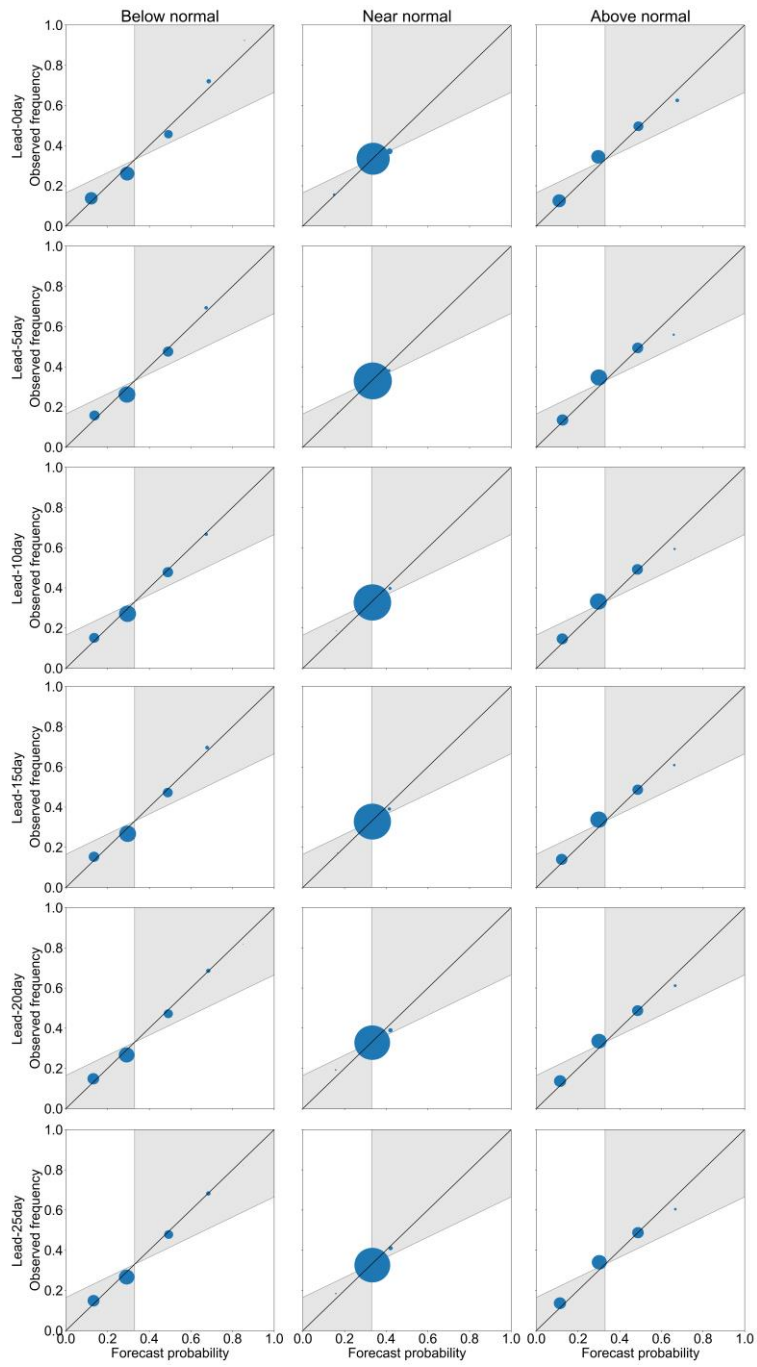


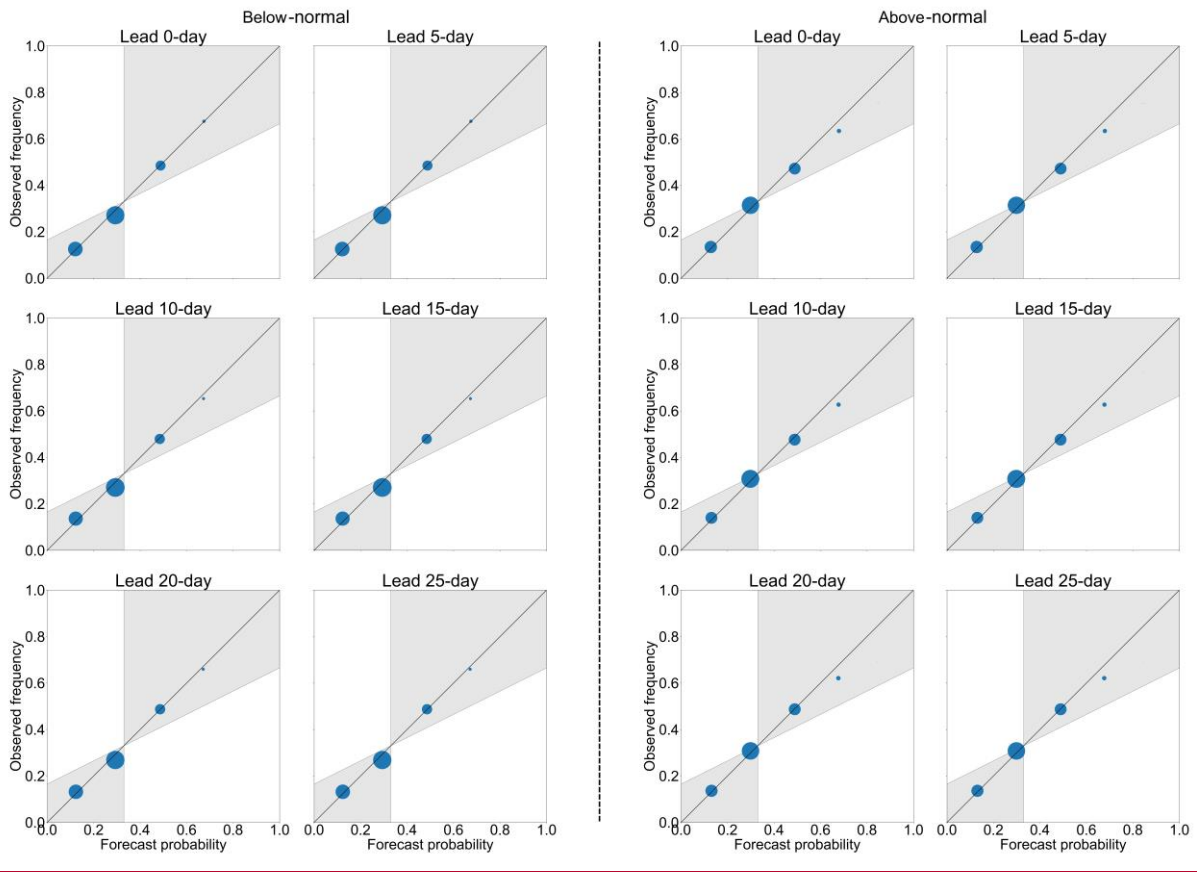
**Figure 7.** The cross-validated CRPS skill scores of the STP-BHM model for pentad mean precipitation amount forecasts with different predictors (U850, U200, OLRA, H850, H500, H200). ALL denotes that the ISO signals of all atmospheric fields are used as predictors.

545

The attribute diagrams of sub-seasonal forecasts of pentad mean precipitation amount for below-normal and above-normal event at different lead times are shown in Figure 68. Most points fall near the 1:1 line for both below-normal and above-normal events and at all lead times, indicating. This suggests that the probabilistic forecast distributions are reliable. The results also suggest that the probabilistic forecasts are sharp at all lead times, especially for below-normal and above-normal categories. However, the forecast probabilities deviate slightly from the 1:1 line at higher forecast probabilities for above-normal event, indicating that the sharpness for above-normal event should be further improved.

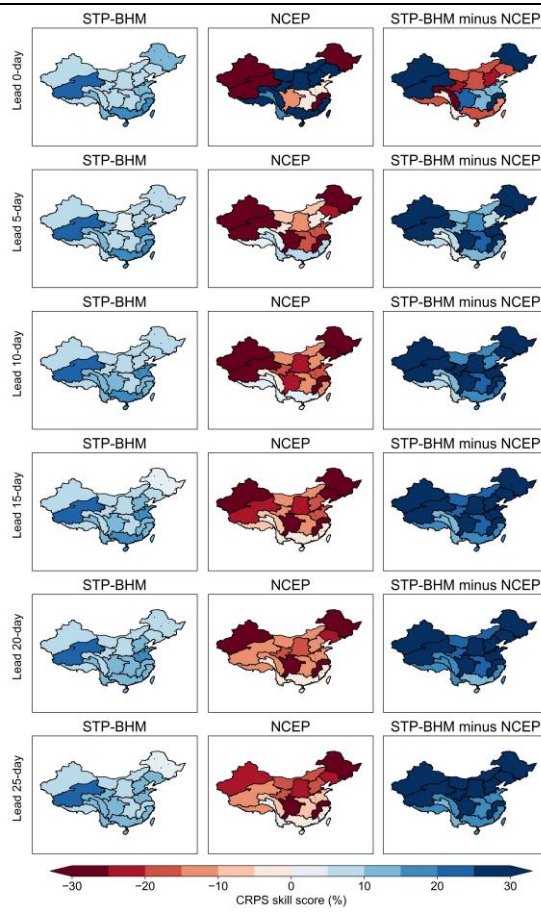
550





555 **Figure 6-Attribute 8.** The attribute diagram of the STP-BHM model for the prediction of below-normal and above-normal events of pentad mean precipitation forecasts during the boreal summer monsoon for tercile based categories amount at different lead times. Forecast probability is binned with width of 0.2, and the size of each dot represents the dots indicates fraction of forecasts that fall into a particular probability bin.

560 Figure 9 compares the sharpness of CRPS skill scores of the STP-BHM model and the NCEP model from May to October during the period of 1999~2010. Although the NCEP model is not the top scoring model for sub-seasonal precipitation forecasts, the hindcast frequency of the NCEP model makes it able to generate pentad mean precipitation forecasts for the same period as the STP-BHM model from 1999 to 2010. It is not surprise that the NCEP model outperforms the STP-BHM model when the lead time is within 5 days. However, we should note that the STP-BHM model shows much higher probabilistic forecasts forecast skill compared to the NCEP model at longer lead times. Positive CRPS skill scores are observed for the STP-BHM model over most hydroclimatic regions, whereas the skill scores are mostly negative for the NCEP model.



570

**Figure 9.** The comparison of the CRPS skill scores of the STP-BHM model and the NCEP model during the period of 1999~2010 from May to October.

### **3.2 Forecast skill of pentad mean precipitation anomalies**

575

The cross-validated CRPS skill scores for sub-seasonal forecasts of pentad mean precipitation anomalies are shown in Figure 10. The STP-BHM model shows positive CRPS skill scores over most hydroclimatic regions, except Inland rivers in Xinjiang (Region 1) and Inland rivers in northern Tibet (Region 2). This may be explained by the relatively lower variability of pentad mean precipitation anomalies in these regions. In addition, the STP-BHM model shows higher forecast skill in eastern China with CRPS skill scores range from 10% to 15%. In comparison, the forecast skill in Inland Rivers in Inner Mongolia (Region 3), Upper Yellow River (Region 5), Upper Yangtze River (Region 9), Southwest rivers in southern Tibet (Region 11), Southwest rivers in Yunnan (Region 12), Yangtze River (Region 13), and Pearl River (Region 16) are lower. Similar results are also found by Zhu and Li (2017a), which the southwestern China shows lowest forecast skill compared to other regions.

580

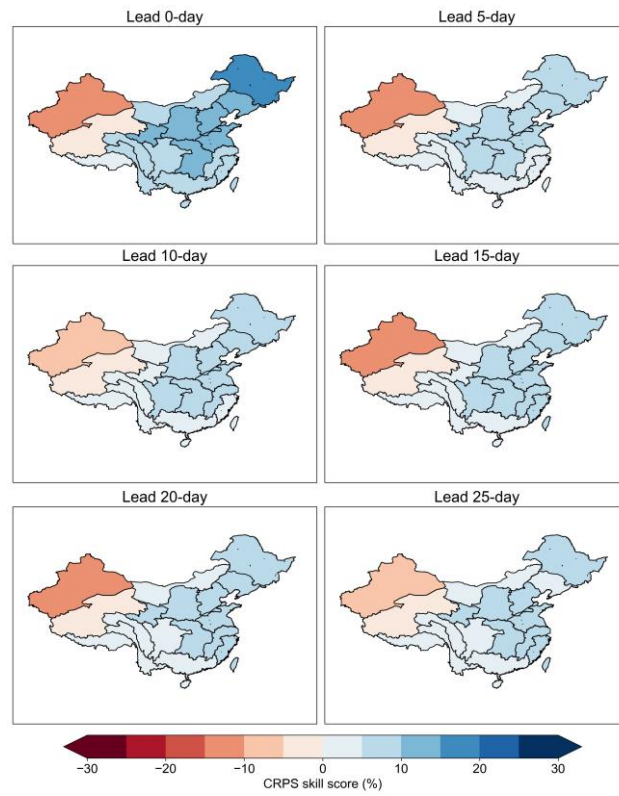


**Figure 10.** Same as Figure 5, but for pentad mean precipitation anomalies.

585

The brier skill scores of pentad mean precipitation anomalies for below-normal and above-normal events are presented in Figure 11. Positive brier skill scores are found over all regions and all lead times, indicating that the STP-BHM model outperforms the cross-validated climatological forecasts for extreme events. Meanwhile, the differences of brier skill scores in different hydroclimatic regions are small, where the brier skill scores are mostly ranging from 5%~15% for both below-normal and above-normal events.

590

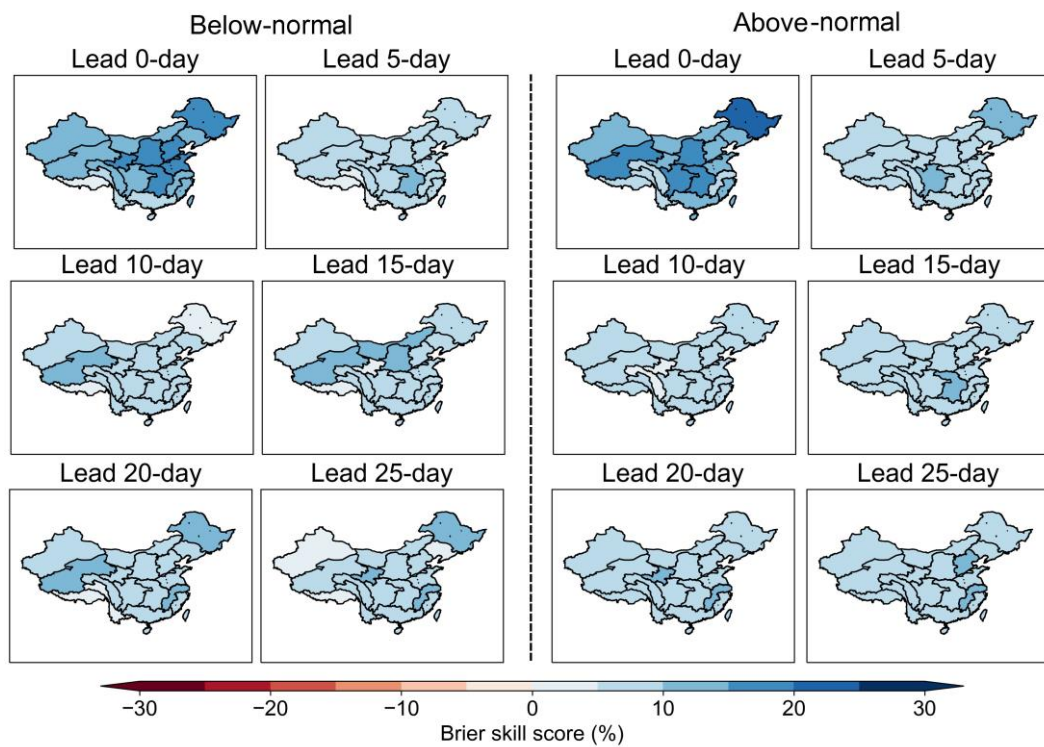


**Figure 11.** Same as Figure 6, but for pentad mean precipitation anomalies.

Figure 12 compares the CRPS skill scores of pentad mean precipitation anomalies with different predictors. Overall, the STP-BHM model with OLRA used as predictor shows higher forecast skill compared to other predictors for almost all hydroclimatic regions and lead times. This suggests that the OLRA contributes most to the overall forecast skill of pentad mean precipitation anomalies.

595

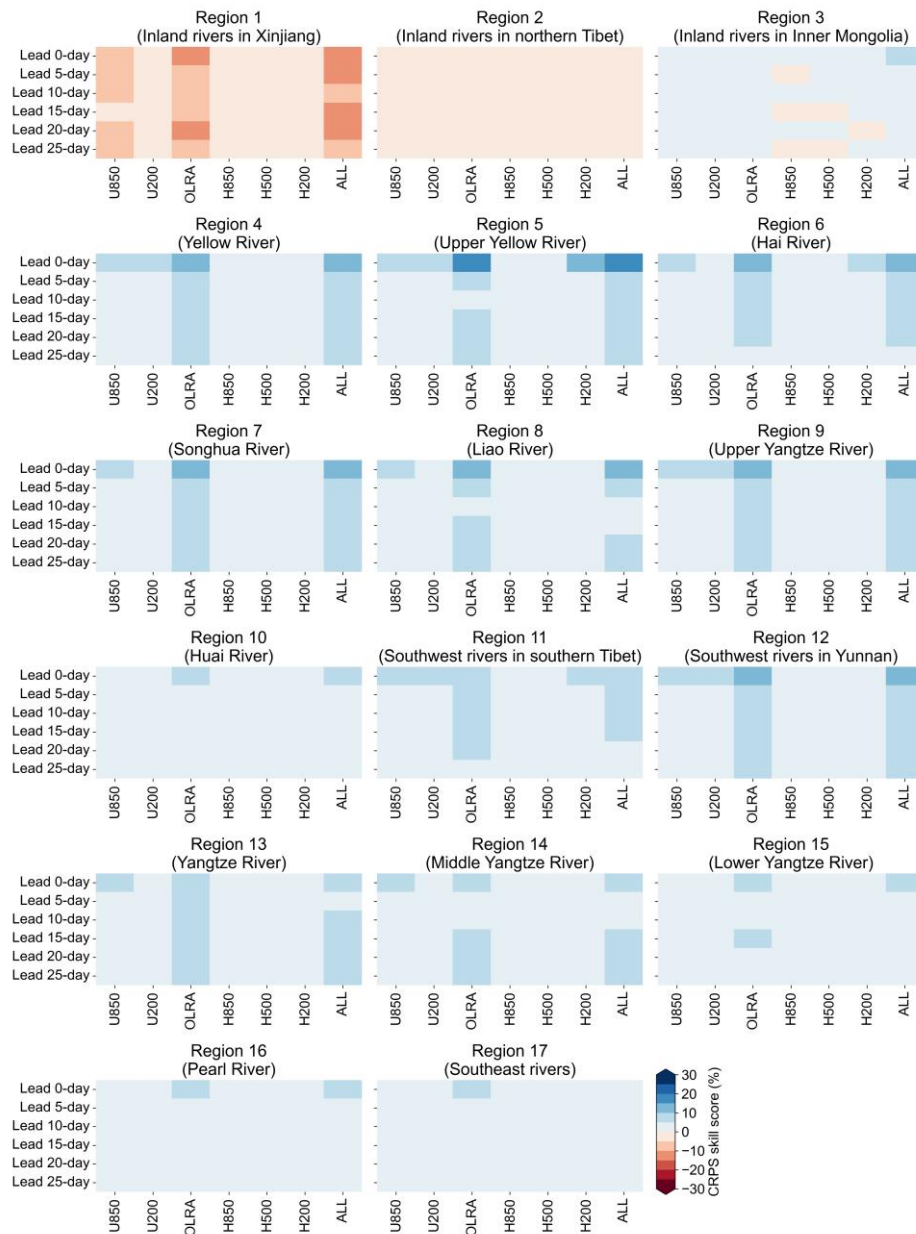


**Figure 12.** Same as Figure 7, but for pentad mean precipitation anomalies.

600

Shown in Figure 13 is the attribute diagram of sub-seasonal forecasts of pentad mean precipitation anomalies for below-normal and above-normal event at different lead times. Most points fall close to the 1:1 line for both below-normal and above-normal events. This suggests that the probabilistic forecast distributions are reliable for pentad mean precipitation anomalies as well. The sharpness of STP-BHM model is also observed especially for below-normal event.

605

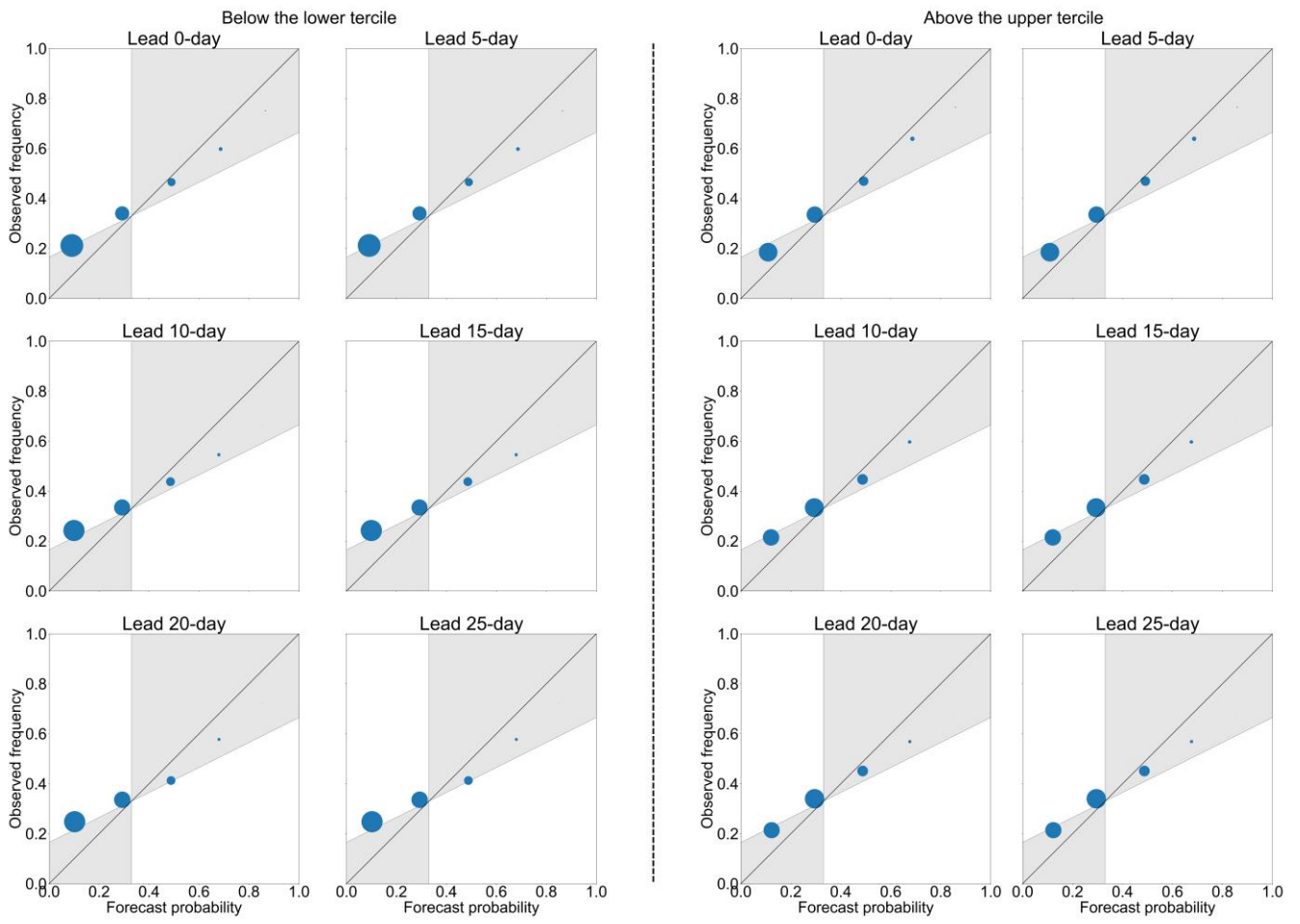


**Figure 13.** Same as Figure 8, but for pentad mean precipitation anomalies.

## 4. Discussion

### 610 4.1 Forecast skill and possible mechanism

In this study, we first ~~define potential predictors by analyzing~~ analyze the ~~relations~~ relationship between ~~pentad mean precipitation and preceding 10-60 day ISO large-scale circulation signals. Robust predictors of atmospheric fields and precipitation. The coupled patterns are identified using the Lasso regression~~ extracted and ~~stepwise regression approaches. the~~ corresponding projection coefficients are defined as predictors. A Bayesian hierarchical model is then established and applied to predict ~~sub-seasonal precipitation for each hydroclimatic region. Our results demonstrate that the Bayesian hierarchical model could provide skillful deterministic sub-seasonal~~ both pentad mean precipitation amount and pentad mean precipitation anomalies over China. Our results suggest that the STP-BHM model can provide skillful and reliable probabilistic forecasts over southeastern and southwestern for both pentad mean precipitation amount and pentad mean precipitation anomalies at a lead of 20-25 days over most hydroclimatic regions in China. However, the



~~deterministic predictive skills over northeastern China are much lower. The decomposition of KGE values~~spatial patterns of skill scores suggest that the ~~intraseasonal variability~~STP-BHM model is ~~underestimated in these regions~~more skillful over southern China. This may be explained by the different characteristics of intraseasonal variability and different possible mechanism over different hydroclimatic regions. Wang (2007) analyzed the precipitation variability from April to September over China, and the results suggested that the seasonal component accounted for nearly 70% of the total variability over northeastern China. The intraseasonal (10-90 days) component only accounted for nearly 7% of the total variability, which indicate that the intraseasonal precipitation over these regions have no significant frequency peak. In comparison, the sub-seasonal component accounted for over 20% of the total variability in southeastern ~~and southwestern~~ China. Ouyang and Liu (2020) also found that the boreal summer monsoon intraseasonal variability of precipitation over the lower Yangtze River basin was mainly dominated by the relatively low-frequency 12-20-day variability and high-frequency 8-12-day variability. Wang and Duan (2015) demonstrated that the Quasi-biweekly oscillation (QBWO, 10-20 days oscillation) was the dominant mode of intraseasonal variability of summer precipitation over the Tibetan Plateau. The relations between atmospheric intraseasonal oscillation and the low-frequency variability of precipitation vary from region to region as well. Ren and Shen (2016) suggested that the impact of tropical atmospheric intraseasonal oscillation on precipitation were more significant in regions in southern China and the Tibetan Plateau areas during the boreal summer. \_

~~Compared to deterministic forecasts, the probabilistic forecasts are more promising, especially at longer lead times. The CRPS skill scores are over 10% in southeastern and southwestern China when the lead time is beyond 10 days. The skill scores still reach a value of over 5% in other hydroclimatic regions. In contrast, the CRPS skill scores of the BJP calibrated sub-seasonal precipitation forecasts were almost 0% at the lead time of 10-30 days (Li et al., 2020). This suggests that the Bayesian hierarchical model could provide useful forecast information at longer lead times when preceding ISO signals are used as predictors. However, we should also note that the highest CRPS skill scores of the Bayesian hierarchical model are lower than 30% when the lead time is between 0-10 days, while that of the calibrated forecasts are over 50%. This indicates that the calibrated forecasts are more skillful for short to medium range precipitation forecasts. We should also note that the CRPS skill scores of the STP-BHM model are lower than NCEP dynamical models at short lead times.~~ The Calibration, Bridging, and Merging (CBaM) method, which makes the best use of GCM outputs, has been proved to be efficient for improving seasonal precipitation over many regions (Strazzo et al., 2019; Schepen and Wang, 2013; Peng et al., 2014). Recently, Specq and Batté (2020) proposed a similar statistical-dynamical approach

to improve sub-seasonal precipitation forecasts over the southwest tropical Pacific. In the future, the statistical forecasts generated from lagged atmospheric indices should be included in the calibrated forecasts to further improve sub-seasonal precipitation forecast ~~skills~~skill.

655

#### 4.2 Limitations and future work

660

665

670

In this study, the ~~potential predictors are identified~~ correlation between ISO signals of atmospheric fields and ~~precipitation is analyzed~~ using the whole record ~~in spite of~~despite the cross-validation strategy used for statistical modelling. This may introduce artificial skill into the ~~models~~model to some extent. However, ~~defining potential predictors~~the correlation analysis for each step of the cross-validation is difficult in practice. ~~The potential predictors were defined by averaging signals in the areas of significant correlations with large extent for each hydroclimatic region and lead time in this study. Nevertheless, this procedure was time consuming. Although we identified the irregular boundaries of significant correlated areas automatically by the Python package scikit-image (Walt et al., 2014), we should note the correlation did not equal causation. We carefully selected potential predictors by analyzing the possible mechanism of sub-seasonal precipitation for each hydroclimatic region and each lead time. In addition, the definition of potential predictors for each step of the cross-validation is likely to yield similar results. Here, we analyzed~~We analyze the spatial patterns of correlations between ~~lagged~~preceding ISO signals of U850 and ~~filtered~~ precipitation over Region 1 at the lead time of 0-day for ~~each step~~the period of the leave-one-year-out cross-validation: 1979-2016 and 1980-2016 (Figure S33). The results ~~showed little~~show small variability ~~compared to~~between the ~~cross-validated~~ correlation ~~patterns shown in Figure 2. The~~and the whole-period correlation. In addition, the cross-validation strategy used in the statistical modelling procedure ~~could~~can also reduce the chance of overfitting (Vehtari and Lampinen, 2002; Delsole and Shukla, 2009).

675

680

Another limitation of this study is the treatment of zero values adopted in the statistical modelling procedure. We ~~treated~~treat the zero values as censored data, which ~~was~~is also referred as “explicit” approach in Mcinerney et al. (2019). Although this treatment performed well in “low-ephemeral” and “mid-ephemeral” catchments, the performance of this “explicit” approach was poor in “high-ephemeral” (> 50% zero flows) catchments. Further development is required to overcome this problem. The copula functions are flexible in choosing marginal distributions, and have been widely used in hydrological simulations in recent years (Zhang and Singh, 2007; Vernieuwe et al., 2015; De Michele and Salvadori, 2003). Compared to the Bayesian

---

statistics we used in this study, the copula functions are more general and the normalization may not be required when the skewed distributions are used as the marginal distribution of precipitation. This may provide a possible solution to overcome the problems caused by the large amount of zero values.

685

We built the Bayesian hierarchical model for each hydroclimatic region separately. However, the spatial patterns of precipitation have not been considered yet. The spatial Bayesian hierarchical model, which ~~is able to~~ capture the spatial dependence of precipitation between different regions, could be used to provide sub-seasonal precipitation forecasts with spatial coherence (Reza Najafi and Moradkhani, 2013; Bracken et al., 2016). An alternative way to reconstruct the spatial patterns of probabilistic precipitation forecasts is to use the Schaake Shuffle method or Ensemble Copula Coupling method (Roman et al., 2013; Clark et al., 2004). Higher spatial or temporal resolution of precipitation forecasts are also needed for sub-seasonal streamflow forecasts. However, our previous studies indicated that post-processed daily precipitation forecasts from GCMs are of low accuracy when the lead time is beyond 10-14 days. ~~In this study, the large-scale ISO signals was only used to predict pentad mean precipitation as the daily precipitation noise was too large. (Li et al., 2020). In this study, the large-scale ISO signals are only used to predict pentad mean precipitation as the noise of daily precipitation is too large.~~ Spatial or temporal disaggregation may be required in the future to provide daily precipitation forecasts as inputs for hydrological models.

690

695

## 700 5. Conclusions

~~Sub~~Accurate and reliable sub-seasonal precipitation forecasts are difficult as the predictability from atmospheric initialization is lost after two weeks, while the slowly varying boundary conditions do not have substantial impact at such a time scale. The intraseasonal oscillation (ISO) is considered as one of the leading sources of sub-seasonal predictability. However, the ~~relationships~~relationship between ~~ISO~~atmospheric intraseasonal signals and precipitation ~~are~~is of high uncertainty. In this study, we first ~~defined potential predictors by analyzing~~analyze the ~~correlations~~correlation between preceding ~~ISO signals~~atmospheric intraseasonal signals (U850, U200, OLRA, H850, H500, and H200) and precipitation. ~~The spatial-temporal coupled co-variance patterns are constructed for each hydroclimatic region and each lead time. The LASSO and stepwise regression approaches were used to narrow down grid points where the number of potential predictors~~correlation statistically significant at the 5% level. The predictors are then defined by summing the ~~product of the co-variance fields and ISO signals of atmospheric field.~~ A Bayesian hierarchical model ~~was then~~

705

710

established to predict sub-seasonal (BHM) is then built to address the uncertainty in the relationship between the ISO signals of atmospheric fields and precipitation during the boreal summer monsoon season. The posterior distributions of the model parameters are sampled using a Gibbs sampling algorithm. The STP-BHM model is used to predict both pentad mean precipitation amount and pentad mean precipitation anomalies after parameter inference. The performance was evaluated through a leave one-year-out cross-validation strategy for both deterministic and probabilistic forecasts.

Our results suggested that the statistical model we built in this study could provide skillful deterministic sub-seasonal precipitation forecasts over southeastern and southwestern hydroclimatic regions at a lead time of 20-25 days. However, the deterministic forecast skills are much lower over northeastern China, partly owing to the underestimation of intraseasonal variability in these regions. The probabilistic forecasts are more promising, especially at longer lead times. The skill scores and attribute diagrams demonstrated that the statistical model was able to provide skillful and reliable sub-seasonal precipitation forecasts for all hydroclimatic regions from 0-day to 25-day leads compared to climatological forecasts. This suggests that the probabilistic forecasts still could provide useful information by addressing the uncertainties of relationships between ISO signals and precipitation at sub-seasonal time scales. Our results suggest that the STP-BHM model we built in this study can provide skillful and reliable probabilistic forecasts for both pentad mean precipitation amount and pentad mean precipitation anomalies at a lead of 20-25 days over most hydroclimatic regions in China when all ISO signals of atmospheric fields are used as predictors. In addition, the STP-BHM model shows useful predictive skill for below-normal and above-normal events as well, and positive Brier skill scores are observed at all lead times. The spatial patterns of skill scores suggest that the STP-BHM model is more skillful over southern China compared to other regions. The STP-BHM model outperforms the NCEP S2S dynamical model when the lead time is beyond 5 days. To help identify the main sources of sub-seasonal precipitation predictability, we also establish the STP-BHM model for U850, U200, OLRA, H850, H500, and H200, separately. The results suggest that the ISO signals of U850, U200, H850, and H500 contribute more to overall forecast skills for pentad mean precipitation amount predictions. In comparison, the OLRA contributes most to the forecast skill for predictions of pentad mean precipitation anomalies.

In this study, the spatial patterns between ISO signals of

~~In this study, the large-scale circulation ISO signals were extracted from~~ the zonal wind at 850 and 200 hPa,

---

Outgoing Longwave Radiation, and the geopotential height at 850, 500, and 200 hPa-are extracted and used to define predictors. Other sources of sub-seasonal predictability, such as soil moisture, snow cover, and stratosphere-troposphere interaction, ~~could~~will be included in the Bayesian hierarchical model to further improve sub-seasonal precipitation forecasts. The Calibration, Bridging, and Merging (CBaM) method ~~could~~can also be investigated at sub-seasonal time scale to further improve the forecast ~~skills~~skill (Schepen and Wang, 2013; Schepen et al., 2014).

745

#### 750 **Data availability**

The precipitation dataset used in this study can be derived from <http://www.gloh2o.org/mswep/>. The outgoing Longwave radiation (OLR) dataset can be found at <https://www.ncdc.noaa.gov/news/new-outgoing-longwave-radiation-climate-data-record>, and the ERA5 dataset can be sourced from <https://cds.climate.copernicus.eu/>.

#### 755 **Author contribution**

Y.L. and Z.Y. WU designed the experiments and Y.L. carried them out. H.H prepared the data, and H.Y. developed the model code and performed the simulations. Y.L. prepared the manuscript with contributions from all co-authors.

#### 760 **Competing interests**

The authors declare that they have no conflict of interest.

#### **Acknowledgements**

This work was funded by the National Natural Science Foundation of China (Grant ~~number 52009027~~), the ~~Fundamental Research Funds for the Central Universities (Grant number 2019B10214~~numbers: 52009027, U2240225).

765

---

## References

- Abbot, J. and Marohasy, J.: Input selection and optimisation for monthly rainfall forecasting in Queensland, Australia, using artificial neural networks, *Atmospheric Research*, 138, 166-178, 2014.
- 770 Annamalai, H. and Slingo, J. M.: Active/break cycles: diagnosis of the intraseasonal variability of the Asian Summer Monsoon, *Climate Dynamics*, 18, 85-102, 10.1007/s003820100161, 2001.
- Barnston, A. G. and Smith, T. M.: Specification and Prediction of Global Surface Temperature and Precipitation from Global SST Using CCA, *Journal of Climate*, 9, 2660-2697, 10.1175/1520-0442(1996)009<2660:SAPOGS>2.0.CO;2, 1996.
- 775 Beck, H. E., Wood, E. F., Pan, M., Fisher, C. K., Miralles, D. G., van Dijk, A. I. J. M., McVicar, T. R., and Adler, R. F.: MSWEP V2 Global 3-Hourly 0.1° Precipitation: Methodology and Quantitative Assessment, *Bulletin of the American Meteorological Society*, 100, 473-500, 10.1175/BAMS-D-17-0138.1, 2019.
- Bracken, C., Rajagopalan, B., Cheng, L., Kleiber, W., and Gangopadhyay, S.: Spatial Bayesian hierarchical modeling of precipitation extremes over a large domain, *Water Resources Research*, 52, 6643-6655, 780 <https://doi.org/10.1002/2016WR018768>, 2016.
- Brooks, S. P. and Gelman, A.: General methods for monitoring convergence of iterative simulations, *Journal of computational and graphical statistics*, 7, 434-455, 1998.
- Chen, ~~G.~~ and Wang, ~~B.~~: ~~Diversity of the Boreal Summer Intraseasonal Oscillation, *Journal of Geophysical Research: Atmospheres*, 126, e2020JD034137, <https://doi.org/10.1029/2020JD034137>, 2021.~~
- 785 ~~Chen,~~ T.-C., Wang, S.-Y., Huang, W.-R., and Yen, M.-C.: Variation of the East Asian Summer Monsoon Rainfall, *Journal of Climate*, 17, 744-762, 10.1175/1520-0442(2004)017<0744:VOTEAS>2.0.CO;2, 2004.
- Chen, X., Hao, Z., Devineni, N., and Lall, U.: Climate information based streamflow and rainfall forecasts for Huai River basin using hierarchical Bayesian modeling, *Hydrology and Earth System Sciences*, 18, 1539-1548, 2014.
- 790 ~~Chu,~~ ~~H.~~, ~~Wei,~~ ~~J.~~, and ~~Wu,~~ ~~W.~~: ~~Streamflow prediction using LASSO-FCM-DBN approach based on hydro-meteorological condition classification, *Journal of Hydrology*, 580, 10.1016/J.JHYDROL.2019.124253, 2020.~~
- ~~Chu,~~ P.-S. and Zhao, X.: A Bayesian Regression Approach for Predicting Seasonal Tropical Cyclone Activity over the Central North Pacific, *Journal of Climate*, 20, 4002-4013, 10.1175/JCLI4214.1, 2007.
- 795 Clark, M., Gangopadhyay, S., Hay, L., Rajagopalan, B., and Wilby, R.: The Schaake Shuffle: A Method for Reconstructing Space-Time Variability in Forecasted Precipitation and Temperature Fields, *Journal of*

---

Hydrometeorology, 5, 243-262, 10.1175/1525-7541(2004)005<0243:TSSAMF>2.0.CO;2, 2004.

de Andrade, F. M., Coelho, C. A., and Cavalcanti, I. F.: Global precipitation hindcast quality assessment of the Subseasonal to Seasonal (S2S) prediction project models, *Climate dynamics*, 52, 5451-5475, 2019.

800 De Michele, C. and Salvadori, G.: A Generalized Pareto intensity-duration model of storm rainfall exploiting 2-Copulas, *Journal of Geophysical Research: Atmospheres*, 108, <https://doi.org/10.1029/2002JD002534>, 2003.

DelSole, T. and Shukla, J.: Artificial Skill due to Predictor Screening, *Journal of Climate*, 22, 331-345, 10.1175/2008JCLI2414.1, 2009.

805 Denwood, M. J.: runjags: An R Package Providing Interface Utilities, Model Templates, Parallel Computing Methods and Additional Distributions for MCMC Models in JAGS., *Journal of Statistical Software*, 71, 1-25, 10.18637/jss.v071.i09, 2016.

Devineni, N., Lall, U., Pederson, N., and Cook, E.: A Tree-Ring-Based Reconstruction of Delaware River Basin Streamflow Using Hierarchical Bayesian Regression, *Journal of Climate*, 26, 4357-4374, 10.1175/JCLID-11-00675.1, 2013.

810 Duchon, C. E.: Lanczos Filtering in One and Two Dimensions, *Journal of Applied Meteorology and Climatology*, 18, 1016-1022, 10.1175/1520-0450(1979)018<1016:LFIOAT>2.0.CO;2, 1979.

Eden, J. M., van Oldenborgh, G. J., Hawkins, E., and Suckling, E. B.: A global empirical system for probabilistic seasonal climate prediction, *Geosci. Model Dev.*, 8, 3947-3973, 10.5194/gmd-8-3947-2015, 2015.

815 Gelman, A. and Hill, J.: *Data analysis using regression and multilevel/hierarchical models*, Cambridge university press 2006.

Gerlitz, L., Vorogushyn, S., Apel, H., Gafurov, A., Unger-Shayesteh, K., and Merz, B.: A statistically based seasonal precipitation forecast model with automatic predictor selection and its application to central and south Asia, *hydrology and earth system sciences*, 20, 4605-4623, 10.5194/HESS-20-4605-2016, 2016.

820 ~~Gupta, H. V., Kling, H., Yilmaz, K. K., and Martinez, G. F.: Decomposition of the mean squared error and NSE performance criteria: Implications for improving hydrological modelling, *Journal of Hydrology*, 377, 80-91, <https://doi.org/10.1016/j.jhydrol.2009.08.003>, 2009.~~

~~Hammami, D., Lee, T. S., Ouarda, T. B. M. J., and Lee, J.: Predictor selection for downscaling GCM data with LASSO, *Journal of Geophysical Research: Atmospheres*, 117, <https://doi.org/10.1029/2012JD017864>, 2012.~~

825 Hersbach, H., Bell, B., Berrisford, P., Hirahara, S., Horányi, A., Muñoz-Sabater, J., Nicolas, J., Peubey, C.,

---

Radu, R., and Schepers, D.: The ERA5 global reanalysis, *Quarterly Journal of the Royal Meteorological Society*, 146, 1999-2049, 2020.

Hsu, P.-c., Zang, Y., Zhu, Z., and Li, T.: [Subseasonal-to-seasonal\(S2S\) prediction using the spatial-temporal projection model \(STPM\), \*Transactions of Atmospheric Sciences\*, 43, 212-224, 2020.](#)

830 [Hsu, P.-C., Li, T., You, L., Gao, J., and Ren, H.-L.: A spatial–temporal projection model for 10–30 day rainfall forecast in South China, \*Climate Dynamics\*, 44, 1227-1244, 10.1007/s00382-014-2215-4, 2015.](#)

Hsu, W.-r. and Murphy, A. H.: The attributes diagram A geometrical framework for assessing the quality of probability forecasts, *International Journal of Forecasting*, 2, 285-293, 1986.

835 Hwang, S.-O., Schemm, J.-K. E., Barnston, A. G., and Kwon, W.-T.: Long-Lead Seasonal Forecast Skill in Far Eastern Asia Using Canonical Correlation Analysis, *Journal of Climate*, 14, 3005-3016, 10.1175/1520-0442(2001)014<3005:LLSFSI>2.0.CO;2, 2001.

Jia, X., Chen, L., Ren, F., and Li, C.: Impacts of the MJO on winter rainfall and circulation in China, *Advances in Atmospheric Sciences*, 28, 521-533, 10.1007/s00376-010-9118-z, 2011.

840 Kirono, D. G., Chiew, F. H., and Kent, D. M.: Identification of best predictors for forecasting seasonal rainfall and runoff in Australia, *Hydrological Processes*, 24, 1237-1247, 2010.

[Kling, H., Fuchs, M., and Paulin, M.: Runoff conditions in the upper Danube basin under an ensemble of climate change scenarios, \*Journal of Hydrology\*, 424-425, 264-277, <https://doi.org/10.1016/j.jhydrol.2012.01.011>, 2012.](#)

845 Lang, Y., Ye, A., Gong, W., Miao, C., Di, Z., Xu, J., Liu, Y., Luo, L., and Duan, Q.: Evaluating Skill of Seasonal Precipitation and Temperature Predictions of NCEP CFSv2 Forecasts over 17 Hydroclimatic Regions in China, *Journal of Hydrometeorology*, 15, 1546-1559, 10.1175/JHM-D-13-0208.1, 2014.

Lee, J.-Y., Wang, B., Wheeler, M. C., Fu, X., Waliser, D. E., and Kang, I.-S.: Real-time multivariate indices for the boreal summer intraseasonal oscillation over the Asian summer monsoon region, *Climate Dynamics*, 40, 493-509, 10.1007/s00382-012-1544-4, 2013.

850 Lepore, C., Tippet, M. K., and Allen, J. T.: ENSO-based probabilistic forecasts of March–May U.S. tornado and hail activity, *Geophysical Research Letters*, 44, 9093-9101, <https://doi.org/10.1002/2017GL074781>, 2017.

Leung, J. C.-H. and Qian, W.: Monitoring the Madden–Julian oscillation with geopotential height, *Climate Dynamics*, 49, 1981-2006, 10.1007/s00382-016-3431-x, 2017.

855 [Li, W., Hsu, P.-c., He, J., Zhu, Z., and Zhang, W.: Extended range forecast of spring rainfall in southern China](#)



~~based on the Madden-Julian Oscillation, *Meteorology and Atmospheric Physics*, 128, 331-345, 10.1007/s00703-015-0418-9, 2016.~~

860 ~~Li, Y., Wu, Z., He, H., Wang, Q. J., Xu, H., and Lu, G.: Post-processing sub-seasonal precipitation forecasts at various spatiotemporal scales across China during boreal summer monsoon, *Journal of Hydrology*, 125742, 2020.~~

Lima, C. H. R. and Lall, U.: Hierarchical Bayesian modeling of multisite daily rainfall occurrence: Rainy season onset, peak, and end, *Water resources research*, 45, 2009.

Lima, C. H. R. and Lall, U.: Spatial scaling in a changing climate: A hierarchical bayesian model for non-stationary multi-site annual maximum and monthly streamflow, *Journal of Hydrology*, 383, 307-318, 2010.

865 Livezey, R. E. and Chen, W. Y.: Statistical Field Significance and its Determination by Monte Carlo Techniques, *Monthly Weather Review*, 111, 46-59, 10.1175/1520-0493(1983)111<0046:SFSAID>2.0.CO;2, 1983.

Lü, A., Jia, S., Zhu, W., Yan, H., Duan, S., and Yao, Z.: El Niño-Southern Oscillation and water resources in the headwaters region of the Yellow River: links and potential for forecasting, *Hydrology and Earth System Sciences*, 15, 1273-1281, 2011.

870 Madden, R. A. and Julian, P. R.: Detection of a 40–50 Day Oscillation in the Zonal Wind in the Tropical Pacific, *Journal of Atmospheric Sciences*, 28, 702-708, 10.1175/1520-0469(1971)028<0702:Doadoi>2.0.Co;2, 1971.

Madden, R. A. and Julian, P. R.: Description of Global-Scale Circulation Cells in the Tropics with a 40–50 Day Period, *Journal of Atmospheric Sciences*, 29, 1109-1123, 10.1175/1520-0469(1972)029<1109:DOGSCC>2.0.CO;2, 1972.

875 McInerney, D., Kavetski, D., Thyer, M., Lerat, J., and Kuczera, G.: Benefits of Explicit Treatment of Zero Flows in Probabilistic Hydrological Modeling of Ephemeral Catchments, *Water Resources Research*, 55, 11035-11060, <https://doi.org/10.1029/2018WR024148>, 2019.

~~McNeish, D. M.: Using Lasso for Predictor Selection and to Assuage Overfitting: A Method Long Overlooked in Behavioral Sciences, *Multivariate Behavioral Research*, 50, 471-484, 10.1080/00273171.2015.1036965, 2015.~~

880 Mekanik, F., Imteaz, M., Gato-Trinidad, S., and Elmahdi, A.: Multiple regression and Artificial Neural Network for long-term rainfall forecasting using large scale climate modes, *Journal of Hydrology*, 503, 11-21, 2013.

885 Michaelsen, J.: Cross-Validation in Statistical Climate Forecast Models, *Journal of Applied Meteorology and Climatology*, 26, 1589-1600, 10.1175/1520-0450(1987)026<1589:CVISCF>2.0.CO;2, 1987.

---

~~Nardi, Y. and Rinaldo, A.: Autoregressive process modeling via the Lasso procedure, Journal of Multivariate Analysis, 102, 528-549, <https://doi.org/10.1016/j.jmva.2010.10.012>, 2011.~~

- 890 Ouyang, Y. and Liu, F.: Intraseasonal variability of summer monsoon rainfall over the lower reaches of the Yangtze River basin, Atmospheric and Oceanic Science Letters, 13, 323-329, 10.1080/16742834.2020.1741322, 2020.
- Peel, M. C., Finlayson, B. L., and McMahon, T. A.: Updated world map of the Köppen-Geiger climate classification, Hydrol. Earth Syst. Sci., 11, 1633-1644, 10.5194/hess-11-1633-2007, 2007.
- 895 Pegion, K., Kirtman, B. P., Becker, E., Collins, D. C., LaJoie, E., Burgman, R., Bell, R., DelSole, T., Min, D., and Zhu, Y.: The Subseasonal Experiment (SubX): A multimodel subseasonal prediction experiment, Bulletin of the American Meteorological Society, 100, 2043-2060, 2019.
- Peng, Z., Wang, Q. J., Bennett, J. C., Pokhrel, P., and Wang, Z.: Seasonal precipitation forecasts over China using monthly large-scale oceanic-atmospheric indices, journal of hydrology, 519, 792-802, 10.1016/J.JHYDROL.2014.08.012, 2014.
- 900 Ren, H. and Shen, Y.: A New Look at Impacts of MJO on Weather and Climate in China (in Chinese), Advances in Meteorological Science and Technology, 6, 97-105, 2016.
- Renard, B.: A Bayesian hierarchical approach to regional frequency analysis, Water Resources Research, 47, <https://doi.org/10.1029/2010WR010089>, 2011.
- Reza Najafi, M. and Moradkhani, H.: Analysis of runoff extremes using spatial hierarchical Bayesian modeling, Water Resources Research, 49, 6656-6670, <https://doi.org/10.1002/wrcr.20381>, 2013.
- 905 Robertson, A. and Vitart, F.: Sub-seasonal to Seasonal Prediction: The Gap Between Weather and Climate Forecasting, Elsevier2018.
- Roman, S., Thordis, L. T., and Tilmann, G.: Uncertainty Quantification in Complex Simulation Models Using Ensemble Copula Coupling, Statistical Science, 28, 616-640, 10.1214/13-STS443, 2013.
- 910 Schepen, A. and Wang, Q. J.: Toward Accurate and Reliable Forecasts of Australian Seasonal Rainfall by Calibrating and Merging Multiple Coupled GCMs, Monthly Weather Review, 141, 4554-4563, 10.1175/MWR-D-12-00253.1, 2013.
- Schepen, A., Wang, Q. J., and Robertson, D.: Evidence for Using Lagged Climate Indices to Forecast Australian Seasonal Rainfall, Journal of Climate, 25, 1230-1246, 10.1175/jcli-d-11-00156.1, 2012.
- 915 Schepen, A., Wang, Q. J., and Robertson, D. E.: Seasonal Forecasts of Australian Rainfall through Calibration and Bridging of Coupled GCM Outputs, Monthly Weather Review, 142, 1758-1770, 10.1175/MWR-D-13-

---

00248.1, 2014.

- Schepen, A., Zhao, T., Wang, Q. J., and Robertson, D. E.: A Bayesian modelling method for post-processing daily sub-seasonal to seasonal rainfall forecasts from global climate models and evaluation for 12 Australian catchments, *Hydrology Earth System Sciences*, 22, 1615-1628, 2018.
- 920 Sohrabi, S., Brissette, F. P., and Arsenault, R.: Coupling large-scale climate indices with a stochastic weather generator to improve long-term streamflow forecasts in a Canadian watershed, *Journal of Hydrology*, 594, 125925, <https://doi.org/10.1016/j.jhydrol.2020.125925>, 2021.
- Specq, D. and Batté, L.: Improving subseasonal precipitation forecasts through a statistical–dynamical approach : application to the southwest tropical Pacific, *Climate Dynamics*, 55, 1913-1927, 925 10.1007/s00382-020-05355-7, 2020.
- Strazzo, S., Collins, D. C., Schepen, A., Wang, Q. J., Becker, E., and Jia, L.: Application of a Hybrid Statistical?Dynamical System to Seasonal Prediction of North American Temperature and Precipitation, *Monthly Weather Review*, 147, 607-625, 10.1175/MWR-D-18-0156.1, 2019.
- Totz, S., Tziperman, E., Coumou, D., Pfeiffer, K., and Cohen, J.: Winter Precipitation Forecast in the European 930 and Mediterranean Regions Using Cluster Analysis, *Geophysical Research Letters*, 44, 12,418-412,426, <https://doi.org/10.1002/2017GL075674>, 2017.
- Tuel, A. and Eltahir, E. A. B.: Seasonal Precipitation Forecast Over Morocco, *Water Resources Research*, 54, 9118-9130, <https://doi.org/10.1029/2018WR022984>, 2018.
- Vehtari, A. and Lampinen, J.: Bayesian Model Assessment and Comparison Using Cross-Validation Predictive 935 Densities, *Neural Computation*, 14, 2439-2468, 10.1162/08997660260293292, 2002.
- Vernieuwe, H., Vandenberghe, S., De Baets, B., and Verhoest, N. E. C.: A continuous rainfall model based on vine copulas, *Hydrol. Earth Syst. Sci.*, 19, 2685-2699, 10.5194/hess-19-2685-2015, 2015.
- Vigaud, N., Tippett, M. K., Yuan, J., Robertson, A. W., and Acharya, N.: Spatial Correction of Multimodel Ensemble Subseasonal Precipitation Forecasts over North America Using Local Laplacian Eigenfunctions, 940 *Monthly Weather Review*, 148, 523-539, 10.1175/MWR-D-19-0134.1, 2020.
- Vitart, F. and Robertson, A. W.: The sub-seasonal to seasonal prediction project (S2S) and the prediction of extreme events, *npj Climate Atmospheric Science*, 1, 1-7, 2018.
- Vitart, F., Ardilouze, C., Bonet, A., Brookshaw, A., Chen, M., Codorean, C., Déqué, M., Ferranti, L., Fucile, E., and Fuentes, M.: The subseasonal to seasonal (S2S) prediction project database, *Bulletin of the American* 945 *Meteorological Society*, 98, 163-173, <https://doi.org/10.1175/BAMS-D-16-0017.1>, 2017.

- 
- Vitart, F., Robertson, A., Kumar, A., Hendon, H., Takaya, Y., Lin, H., Arribas, A., Lee, J., Waliser, D., and Kirtman, B.: Subseasonal to seasonal prediction: Research implementation plan, WWRP/THORPEX-WCRP Report, 2012.
- ~~Walt, S. v. d., JL, S., J, N., I., F, B., JD, W., N, Y., E, G., T, Y., and contributors, t. s. i.: scikit-image: image processing in Python, PeerJ, 2, <https://doi.org/10.7717/peerj.453>, 2014.~~
- 950 Wang, B. and Xie, X.: A Model for the Boreal Summer Intraseasonal Oscillation, *Journal of the Atmospheric Sciences*, 54, 72-86, 10.1175/1520-0469(1997)054<0072:AMFTBS>2.0.CO;2, 1997.
- Wang, M. and Duan, A.: Quasi-Biweekly Oscillation over the Tibetan Plateau and Its Link with the Asian Summer Monsoon, *Journal of Climate*, 28, 4921-4940, 10.1175/JCLI-D-14-00658.1, 2015.
- 955 Wang, Q. J., Robertson, D. E., and Chiew, F. H. S.: A Bayesian joint probability modeling approach for seasonal forecasting of streamflows at multiple sites, *Water Resources Research*, 45, <https://doi.org/10.1029/2008WR007355>, 2009.
- Wang, Q. J., Shrestha, D. L., Robertson, D. E., and Pokhrel, P.: A log-sinh transformation for data normalization and variance stabilization, *Water Resources Research*, 48, <https://doi.org/10.1029/2011WR010973>, 2012.
- 960 Wang, Z.: Climate variability of summer rainfalls in China and the possible mechanism (in Chinese), *Chinese Academy of Sciences*, 2007.
- Wheeler, M. C. and Hendon, H. H.: An All-Season Real-Time Multivariate MJO Index: Development of an Index for Monitoring and Prediction, *Monthly Weather Review*, 132, 1917-1932, 10.1175/1520-0493(2004)132<1917:AARMMI>2.0.CO;2, 2004.
- 965 Woolnough, S. J.: Chapter 5 - The Madden-Julian Oscillation, in: *Sub-Seasonal to Seasonal Prediction*, edited by: Robertson, A. W., and Vitart, F., Elsevier, 93-117, <https://doi.org/10.1016/B978-0-12-811714-9.00005-X>, 2019.
- Wu, Z., Xu, Z., Wang, F., He, H., Zhou, J., Wu, X., and Liu, Z.: Hydrologic Evaluation of Multi-Source Satellite Precipitation Products for the Upper Huaihe River Basin, China, *Remote Sensing*, 10, 10.3390/rs10060840, 2018.
- 970 Yeo, I. and Johnson, R. A.: A new family of power transformations to improve normality or symmetry, *Biometrika*, 87, 954-959, 2000.
- Zhang, C.: Madden-Julian Oscillation, *Review of Geophysics*, 43, <https://doi.org/10.1029/2004RG000158>, 2005.
- 975 Zhang, L. and Singh, V. P.: Bivariate rainfall frequency distributions using Archimedean copulas, *Journal of*

---

Hydrology, 332, 93-109, <https://doi.org/10.1016/j.jhydrol.2006.06.033>, 2007.

Zhang, L., Wang, B., and Zeng, Q.: Impact of the Madden–Julian Oscillation on Summer Rainfall in Southeast China, *Journal of Climate*, 22, 201-216, 10.1175/2008JCLI1959.1, 2009.

Zhu, Z. and Li, T.: The statistical extended-range (10–30-day) forecast of summer rainfall anomalies over the entire China, *Climate Dynamics*, 48, 209-224, 10.1007/s00382-016-3070-2, ~~2017~~2017a.

Zhu, Z. and Li, T.: Empirical prediction of the onset dates of South China Sea summer monsoon, *Climate Dynamics*, 48, 1633-1645, 10.1007/s00382-016-3164-x, 2017b.

Zhu, Z. and Li, T.: Statistical extended-range forecast of winter surface air temperature and extremely cold days over China, *Quarterly Journal of the Royal Meteorological Society*, 143, 1528-1538, <https://doi.org/10.1002/qj.3023>, 2017c.

Zhu, Z. and Li, T.: Extended-range forecasting of Chinese summer surface air temperature and heat waves, *Climate Dynamics*, 50, 2007-2021, 10.1007/s00382-017-3733-7, 2018.

Zhu, Z., Li, T., Hsu, P.-c., and He, J.: A spatial–temporal projection model for extended-range forecast in the tropics, *Climate Dynamics*, 45, 1085-1098, 10.1007/s00382-014-2353-8, 2015.

980

985

990